Geophys. J. Int. (2009)
doi: 10.1111/j.1365-246X.2009.04480.x

Rock magnetism and palaeomagnetism of the Montalbano Jonico section (Italy): evidence for late diagenetic growth of greigite and implications for magnetostratigraphy

Leonardo Sagnotti,[1] Antonio Cascella,[2] Neri Ciaranfi,[3]
Patrizia Macrì,[1] Patrizia Maiorano,[3] Maria Marino[3] and Jacopo Taddeucci[1]

[1] *Istituto Nazionale di Geofisica e Vulcanologia, Roma, Italy. E-mail: leonardo.sagnotti@ingv.it*
[2] *Istituto Nazionale di Geofisica e Vulcanologia, Pisa, Italy*
[3] *Dipartimento di Geologia e Geofisica, Università di Bari, Italy*

Accepted 2009 December 11. Received 2009 December 10; in original form 2009 July 20

SUMMARY

The Montalbano Jonico (MJ) section, cropping out in Southern Italy, represents a potential candidate to define the Lower/Middle Pleistocene boundary and it has been proposed as a suitable Global Stratotype Section and Point (GSSP) of the Ionian Stage (Middle Pleistocene). The MJ section is the only continuous benthic and planktonic $\delta^{18}O$ on-land reference in the Mediterranean area for the Mid-Pleistocene transition, spanning an interval between about 1240 and 645 ka. Combined biostratigraphy and sapropel chronology, tephra stratigraphy and complete high-resolution benthic and planktonic foraminiferal stable oxygen isotope records already provide a firm chronostratigraphic framework for the MJ section. However, magnetostratigraphy was still required to precisely locate the Brunhes-Matuyama transition and to mark the GSSP for the Ionian stage. We carried out a palaeomagnetic study of a subsection (Ideale section) of the MJ composite section, sampling 61 oriented cores from 56 stratigraphic levels spread over a *ca*. 80-m-thick stratigraphic interval that correlates to the oxygen isotopic stage 19 and should therefore include the Brunhes-Matuyama reversal. The palaeomagnetic data indicate a stable and almost single-component natural remanent magnetization (NRM). A characteristic remanent magnetization (ChRM) was clearly identified by stepwise demagnetization of the NRM. The ChRM declination values vary around 0° and the ChRM inclination around the expected value (59°) for a geocentric axial dipole field at the sampling locality. This result indicates that the section has been remagnetized during the Brunhes Chron. A preliminary study of 27 additional not azimuthally oriented hand samples, collected at various levels from other parts of the MJ composite section, indicates that all the samples are of normal polarity and demonstrates that the remagnetization is widespread across the whole exposed stratigraphic sequence.

A series of specific rock magnetic techniques were then applied to investigate the nature of the main magnetic carrier in the study sediments, and they suggest that the main magnetic mineral in the MJ section is the iron sulphide greigite (Fe_3S_4). Scanning electron microscope observations and elemental microanalysis reveal that greigite occurs both as individual euhedral crystals and in iron sulphides aggregates filling voids in the clay matrix. Therefore, we infer that the remagnetization of the section is due to the late-diagenetic growth of greigite under reducing conditions, most likely resulting in the almost complete dissolution of the original magnetic minerals. Iron sulphide formation in the MJ section can be linked to migration of mineralized fluids. Our inferred timing of the remagnetization associated with greigite growth represents the longest remanence acquisition delay documented in greigite-bearing clays of the Italian peninsula so far.

Key words: Remagnetization.

INTRODUCTION

The Montalbano Jonico (hereinafter MJ) section is relevant for Pleistocene stratigraphy due to its excellent land exposure and stratigraphic continuity from Marine Isotope Stage (MIS) 36 to the beginning of MIS 16 (Ciaranfi *et al.* 2009). It has been recently proposed as the reference section for the upper portion of the Calabrian Stage and for the Global Stratotype Section and Point (GSSP) of the Middle Pleistocene and the base of the Ionian Stage (Ciaranfi *et al.* 1997; Ciaranfi & D'Alessandro 2005; Cita *et al.* 2006, 2008; Cita 2008). Cita *et al.* (2006) explicitly stated that the MJ section 'represents the most suitable boundary stratotype of the Ionian, once provided with a reliable magnetostratigraphy'. The guiding primary criterion of the GSSP of the Middle Pleistocene is the base of the Brunhes Chron (Richmond 1996). The available accurate stratigraphic data set and the astronomical tuning of the MJ section revealed that it spans the time interval between about 1240 and 645 ka (Ciaranfi *et al.* 2009). Therefore, the MJ section includes the Matuyama-Brunhes (M-B) reversal boundary, which is correlated to the MIS 19 (Tauxe *et al.* 1996) and dated to an astronomically calibrated age of *ca*. 781 ka (Lourens *et al.* 2004).

In this study, we aim to precisely locate the position of the M-B reversal boundary and hence the base of the Ionian stage in the MJ section by means of magnetostratigraphy, supported by additional rock magnetic analysis. The palaeomagnetic sampling focused on an 80-m-thick portion (Ideale section) of the MJ composite section that lies just below the volcaniclastic layer V5, $^{39}Ar/^{40}Ar$ dated at 719.5 ± 12.6 ka (Ciaranfi *et al.* 2009). The Ideale section also comprises MIS 19, and largely overlaps with the temporary disappearance (td2, *sensu* Maiorano & Marino 2004) of calcareous nannofossil *Gephyrocapsa omega*, a biostratigraphic event in turn correlated to MIS 19 (Maiorano *et al.* 2004). On the basis of the available stratigraphic constraints and according to the age model of Ciaranfi *et al.* (2009), the Ideale section has an estimated age range of 750–810 ka and thus encompasses the Matuyama-Brunhes (M-B) reversal, whose midpoint was recently dated at *ca*. 789 ka by Quidelleur *et al.* (2003), *ca*. 774 ka by Channell *et al.* (2004), *ca*. 776 ka by Coe *et al.* (2004) and Singer *et al.* (2008). Our results indicate that the natural remanent magnetization (NRM) of the exposed sediments of the MJ section is carried by a late diagenetic population of greigite (Fe_3S_4) grains, which prevents the use of magnetostratigraphy to resolve the position of the M-B reversal boundary. The modes and timing of greigite formation in the Italian fine-grained sediments will finally be briefly reviewed with reference to their implications for magnetostratigraphy.

GEOLOGICAL SETTING AND STRATIGRAPHY OF THE MJ SECTION

The MJ composite section is located in the southern Italian Foredeep (Bradano Trough), between the Apennines Chain to the west and the Apulia Foreland to the east (Fig. 1). It belongs to the 'argille subappennine' unit (Azzaroli 1968) and consists of a coarsening upward sequence from muddy clays to muddy sands which includes nine volcaniclastic layers (Fig. 1). In total, the MJ composite section is about 450 m thick and it has been reconstructed in the field based on eight subhorizontal overlapping partial sections (FG, 5a, VBJ, DF-DFJ, IDEALE, JS, VCT and M) (Fig. 1). The lower part of the composite section (Interval A) is separated from the upper part (Interval B) by a short stratigraphic gap (Ciaranfi *et al.* 2001; Ciaranfi & D'Alessandro 2005) which spans a time interval of ∼19.52 ka (Ciaranfi *et al.* 2009). Nannofossil analysis indicates that the composite section is referable to the small *Gephyrocapsa-Pseudoemiliana lacunosa* zones. The lowermost part is younger than the Last Occurrence (LO) of large *Gephyrocapsa* and the topmost part of the section is older than the LO of *Gephyrocapsa omega* (Ciaranfi *et al.* 1997, 2001; Maiorano *et al.* 2004). Additional biostratigraphic events are the *Globorotalia crassaformis* influx, the First Common Occurrence (FCO) and Last Common Occurrence (LCO) of *Reticulofenestra asanoi*, and the second temporary disappearance (td2, *sensu* Maiorano & Marino 2004) of *G. omega* (Maiorano *et al.* 2004; Joannin 2007; Joannin *et al.* 2008; Ciaranfi *et al.* 2009) (Fig. 2). Sapropel layers have been recognized in the Interval A, based on benthic foraminiferal assemblages and on planktonic $\delta^{18}O$ data (Stefanelli 2003, 2004; Stefanelli *et al.* 2005), and they have been correlated to insolation maxima, referred to as i-cycles, labelled i-86, i-90, i-102, i-104, i-112 according to sapropel stratigraphy available in Mediterranean area (Fig. 2) (de Kaenel *et al.* 1999; Raffi 2002; Maiorano & Marino 2004; Lourens 2004). Benthic and planktonic $\delta^{18}O$ records are available for the whole composite section (Brilli *et al.* 2000; Ciaranfi *et al.* 2001; Stefanelli 2003; Maiorano *et al.* 2004; Stefanelli *et al.* 2005; Ciaranfi *et al.* 2008; Joannin *et al.* 2008) based on analyses of benthic *Cassidulina carinata* and planktonic *Globigerina bulloides*. The trachitic volcaniclastic layer V5 has been dated with $^{39}Ar/^{40}Ar$ at 719.5 ± 12.6 ka (Ciaranfi *et al.* 2009), thus providing an additional stratigraphic constraint. The correlation between the accurate calcareous plankton biostratigraphy, sapropel and oxygen isotope stratigraphy allowed to astronomically calibrate Interval A (Fig. 2); the $\delta^{18}O_{G.\ bulloides}$ record of Montalbano Jonico Interval B has been tuned to the same record from Mediterranean ODP-Site 975 (oxygen isotope chronology of Pierre *et al.* 1999 modified by Lourens 2004) by visual correlation, supported by radiometric age of V5 layer and stratigraphic position of td2 (Fig. 2). This correlation is also sustained by the glacial–interglacial oscillations observed in $\delta^{18}O_{C.\ carinata}$ record of Montalbano Jonico compared with open ocean benthic stacks (Fig. 2).

The sampled Ideale subsection includes the volcaniclastic layers V3 and V4 (Figs 1 and 2). The V4 layer falls in the middle of MIS 19, with an estimated orbitally tuned age of 792.6 ka (Cita *et al.* 2008; Ciaranfi *et al.* 2009) and it should be stratigraphically very close to the M-B reversal transition.

SAMPLING AND METHODS

Palaeomagnetic sampling was performed by in situ drilling using a water-cooled, diamond-head corer. The cores were oriented using a magnetic compass. We collected 61 oriented cores from 56 stratigraphic levels spread over 80 m of the Ideale subsection, with a mean stratigraphic spacing between cores of 1.4 m. Each palaeomagnetic core was cut into standard cylindrical specimens of 25 mm diameter and 22 mm height.

All palaeomagnetic and rock magnetic measurements were carried out at the palaeomagnetic laboratory of the Istituto Nazionale di Geofisica e Vulcanologia in Rome. The NRM of a standard specimen from each core was measured on a 2G Enterprises DC SQUIDs cryogenic magnetometer, installed within a magnetically shielded room. Stepwise demagnetization of the NRM was carried out either by heating the samples in a palaeomagnetic oven or by translating them through a set of three orthogonal alternating field (AF) coils mounted in-line on the 2G Enterprises system.

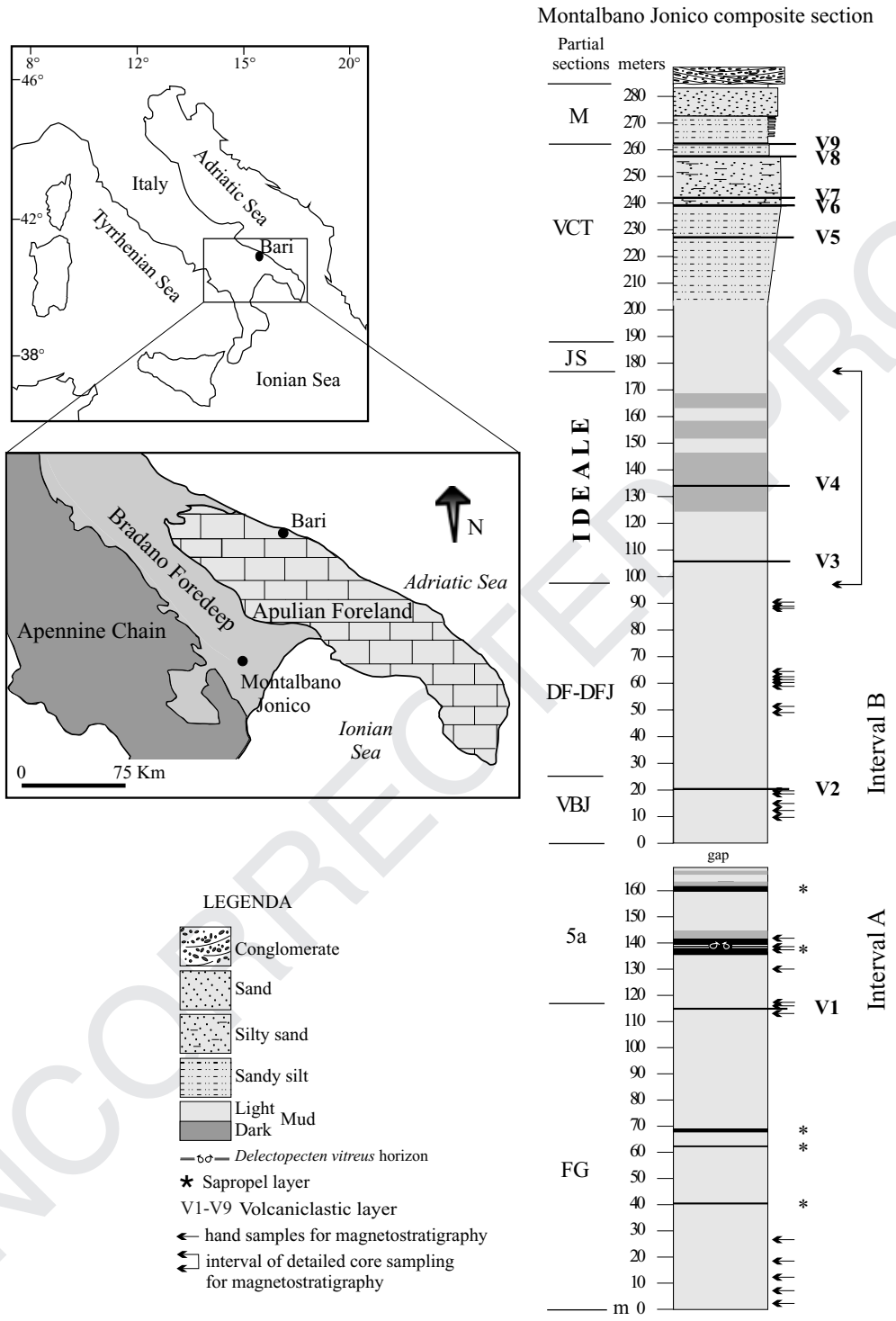

Figure 1. Location map and lithostratigraphy of the Montalbano Jonico composite section.

We first carried out a pilot study on eight pairs of sister specimens collected from distributed stratigraphic levels and subjected these to stepwise thermal (up to 420 °C) and AF (up to 100 mT) demagnetization, until they were fully demagnetized. After each thermal demagnetization step, the magnetic susceptibility (κ) was monitored as a check for thermal alteration. The results indicated that both treatments provide consistent results and allow the clear identification of a characteristic remanent magnetization (ChRM) (Fig. 3). A significant increase in the magnetic susceptibility, indicating production of new magnetic minerals induced by thermal alteration, was observed for all the thermal pilot samples at temperatures higher than 340 °C (Fig. 3). For the AF pilot samples, instead, the acquisition of a spurious gyromagnetic remanent magnetization (GRM) was observed in fields higher than 50–60 mT (Fig. 3). Given that both demagnetization methods allow the unambiguous identification of the same ChRM, we subjected all the remaining samples to AF demagnetization in 12 steps up to a maximum field of 100 mT. This decision relied upon the fact that the AF demagnetization

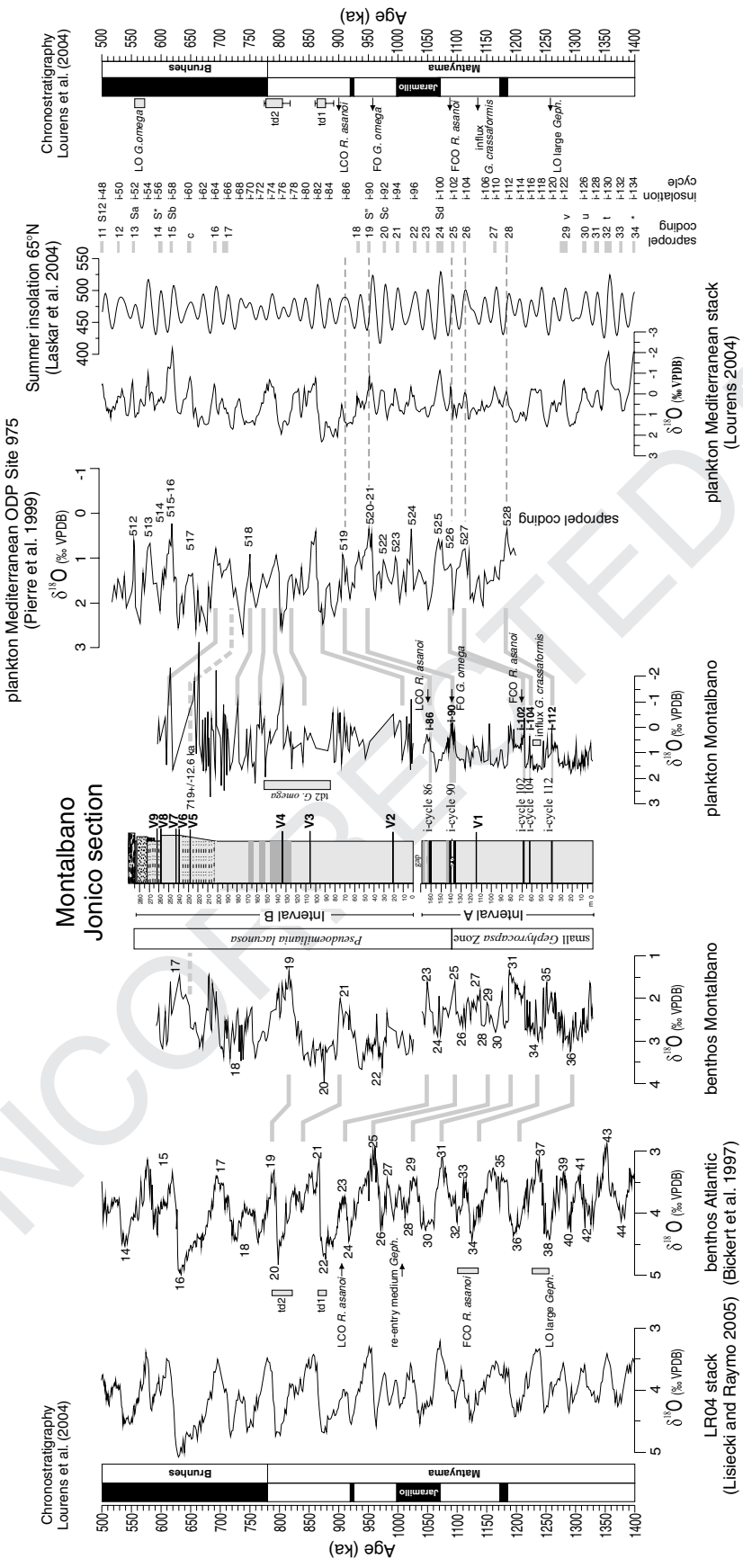

Figure 2. Stratigraphic correlation of Montalbano Jonico benthic and planktonic $\delta^{18}O$ records with the $\delta^{18}O$ Mediterranean and Atlantic Ocean records (modified from Ciaranfi *et al.* 2009). Sapropel coding and sapropel stratigraphy are from Lourens *et al.* (2004) and Lourens (2004). Sapropel coding at Site 957 is from Comas *et al.* (1996) and Murat (1999). FO, first occurrence; LO, last occurrence; FCO, first common occurrence; LCO, last common occurrence; td1 and td2, first and second temporary disappearances of *G. omega*; numbers on oxygen isotope curves are Marine Isotope Stages.

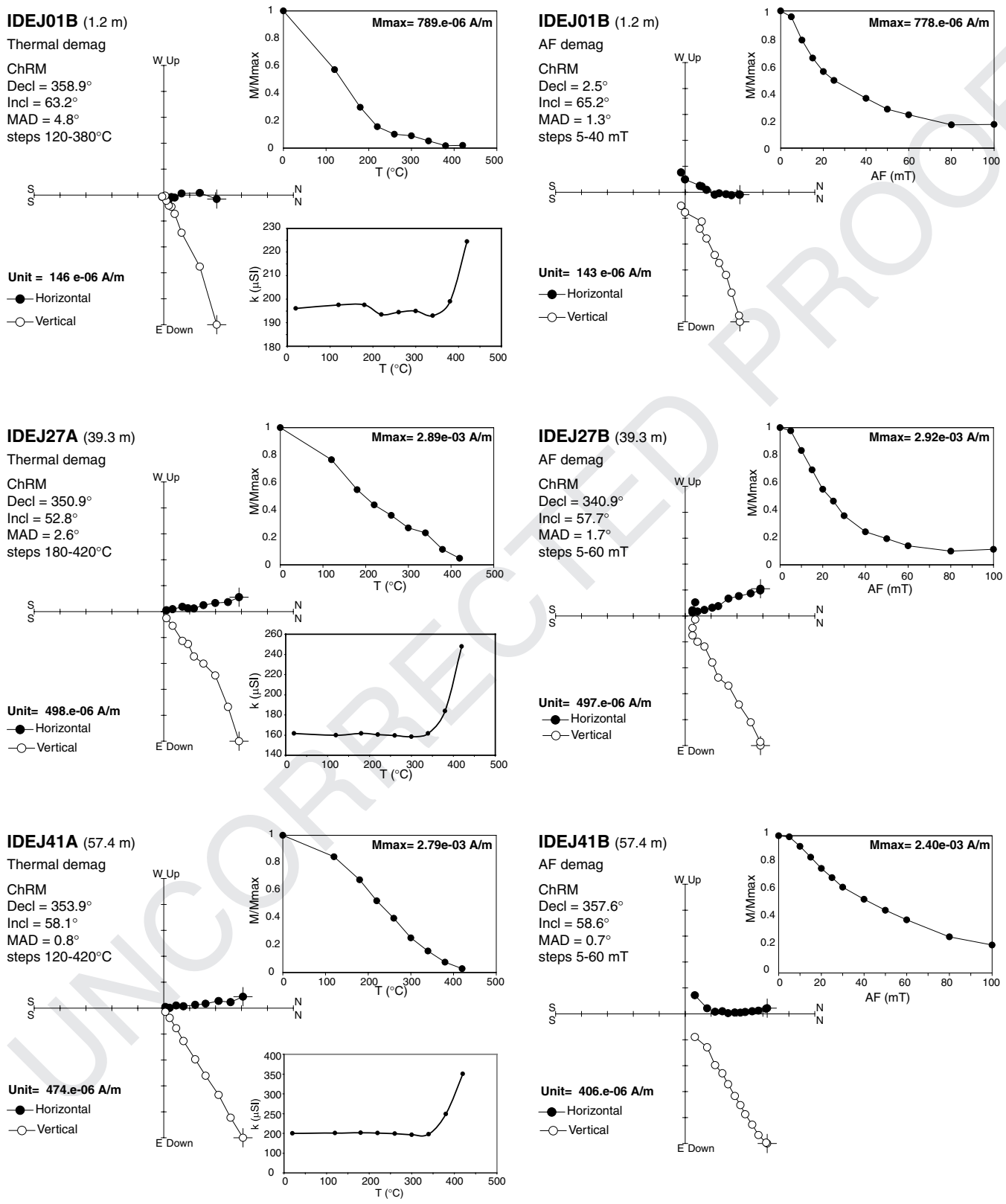

Figure 3. Representative demagnetization plots for three pairs of pilot specimens (from cores IDEJ01, IDEJ27 and IDEJ41). Orthogonal vector diagrams: open and closed symbols represent projections onto vertical and horizontal planes, respectively. The demagnetization data have been visualized and analyzed using the Remasoft program (Chadima & Hrouda 2006). The thermal demagnetization data indicate that the specimens are fully demagnetized at 420 °C. The AF treatment indicates that the samples have a median destructive field of 20–40 mT and acquire a spurious GRM in fields higher than 50–60 mT. The two demagnetization treatments allow the unambiguous identification of the same ChRM, which is defined by linear paths towards the origin in orthogonal vector diagrams.

has the advantages that it can be run in automatic mode and that the demagnetized samples can subsequently be used for further rock magnetic analyses, such as those described below, in contrast to thermal demagnetization where the magnetic mineralogy may be thermally altered upon heating.

In order to identify the nature of the main magnetic carriers, we also carried out a series of rock magnetic experiments on a subset of selected specimens. The rock magnetic measurements included: (1) the stepwise acquisition of an isothermal remanent magnetization (IRM) in 11 distributed standard palaeomagnetic specimens, by applying increasing pulse magnetic fields up to a maximum value of 0.9 T, (2) the stepwise thermal demagnetization of a composite IRM produced by the sequential application of 1.2 T, 0.4 T and 0.12 T pulse fields along the three orthogonal axes of the same 11 cylindrical specimens (according to the method developed by Lowrie 1990) and (3) the measurement of hysteresis properties on small fragments scraped from seven distributed palaeomagnetic specimens. The hysteresis properties were measured on a MicroMag alternating gradient magnetometer (AGM model 2900, Princeton Measurements Corporation) with a maximum applied field of 1 T. From hysteresis cycles, after subtraction of the paramagnetic high-field susceptibility after saturation, we determined the coercive force (B_C), the saturation remanent magnetization (M_{RS}) and the saturation magnetization (M_S). Stepwise acquisition of an isothermal remanent magnetization (IRM) and subsequent DC back-field remagnetization (both in a succession of fields up to 1 T) were also measured on the same fragments with the MicroMag AGM, and the remanent coercive force (B_{CR}) was computed from the back-field remagnetization curves. For a couple of specimens with high magnetic intensity we also analyzed first order reversal curves (FORC). FORCs are a series of partial hysteresis loops made after the sample magnetization is saturated in a large positive applied field, measured by cycling between the positive saturation field and a reversal field B_A. The FORC is defined by the measurement of the magnetization of the sample as a function of an increased field B_B, until positive saturation is reached again (Pike *et al.* 1999; Roberts *et al.* 2000). In this study, 121 FORCs have been measured for each specimen, in steps of 2.8 mT and an averaging time of 500 ms, using a 0.5 T saturating field. The FORC data were then transformed into contour plots, usually referred to as FORC diagrams, by calculating the second derivative of the measured magnetization plotted as a function of B_A and B_B in field space (Pike *et al.* 1999; Roberts *et al.* 2000). The FORC distribution is then rotated counterclockwise by 45°, by defining a new set of coordinates where $B_C = (B_A - B_B)/2$ and $B_U = (B_A + B_B)/2$. The final FORC diagram is a contour plot of $\rho(B_A, B_B)$, drawn using B_C and B_U as the horizontal and vertical axes, respectively. To produce FORC diagrams we used the FORCinel software developed by Harrison & Feinberg (2008). FORCs provide a more complete sampling of the magnetic response of the sample than a single hysteresis loop and the analysis of FORC diagrams allow to define the detailed coercivity distribution of the magnetic particles and their interaction field strengths.

With the aim to reconstruct the magnetic fabric of the studied sediments we also measured the anisotropy of magnetic susceptibility (AMS) of 12 standard cylindrical specimens distributed throughout the Ideal section. The computation of the AMS tensor was carried out following the statistics developed by Jelínek (1978) and using the software Anisoft developed by Chadima & Jelínek (freely distributed by AGICO at http://www.agico.com/software/anisoft/).

Finally, the morphology, texture, and chemical composition of magnetic grains were investigated through observations and analyses carried out with a JEOL JSM 6500F Field Emission (Schottky-type) Scanning Electron Microscope (FE-SEM, resolution 1.5 nm at 15 kV operating voltage), equipped with backscattered electron detector and Energy Dispersion System (EDS, JEOL HYPERNINE, 133 eV resolution) microanalysis. Polished thin sections of the three samples showing the highest κ and NRM intensities (samples IDEJ25, 30 and 50) were carbon-coated and observed at high magnification using both secondary (SE) and backscattered (BSE) electrons. The chemical composition of the particles was characterized by acquiring EDS X-ray spectra (acceleration voltage 10 kV, probe current 0.85 nA), that were converted into standardless chemical analyses with errors less than ±10 per cent relative to the analytical value, as deduced by a comparison with known rock standards. Monte Carlo simulations of the interaction between the electron beam and particle–clay matrix, performed using the CASINO software (Drouin *et al.* 2007), reveal an interaction volume of about 800 nm for our analytical conditions.

RESULTS

Palaeomagnetism

The demagnetization diagrams (Fig. 3) indicate stable palaeomagnetic behaviour throughout the Ideale section, with the demagnetization vectors aligned along linear paths towards the origin, after removal of a viscous low coercivity remanence component at 5–10 mT. A ChRM was clearly determined by principal component analysis (Kirschvink 1980) for 58 specimens from 49 distinct stratigraphic levels. The ChRM direction was computed by fitting a linear component between 5–10 and 50–60 mT, for the specimens demagnetized by AF, and between 120–180 and 380–420 °C, for the specimens thermally demagnetized. The maximum angular deviation (MAD) for each determined ChRM direction was 2° on average, with a full range of variation between 0.5° and 5.5°. As for the AF pilot samples, all the specimens acquired a spurious GRM in AF peaks higher than 40–60 mT. The GRM effects are variably pronounced in the various specimens and may result in a dramatic increase of the remanent magnetization intensity with progression of the AF treatment (e.g. Fig. 4c). We verified that the GRM acquisition is perpendicular to the axis of the magnetometer (i.e. perpendicular to the *Z*-axis of the specimens and to the direction of the last AF demagnetization) and is mostly acquired by the transverse *Y* component. Following the method developed by Fu *et al.* (2008), we computed the ΔGRM/ΔNRM ratio on the *Y* remanence intensity data for all the specimens of the Ideale section. ΔGRM represents the difference of the final intensity measured at the last AF step and the intensity minimum value (MV) during the whole AF treatment and ΔNRM represents the difference of initial intensity value and MV. The ΔGRM/ΔNRM values for the specimens of the Ideale section are mostly comprised between 0.2 and 5, with a full range of variation between 0 and 46.

The ChRM declination and inclination for the samples of the Ideale section indicate that this section is consistently characterized by normal magnetic polarity. The ChRM declination varies around 0° and the ChRM inclination around the expected value (59°) for a geocentric axial dipole field at the sampling locality (Table 1 and Fig. 5). The average palaeomagnetic direction for the Ideale section, as computed by Fisher's statistics (Fisher 1953) was Decl = 355.5°, Incl = 61.3°, with $\alpha_{95} = 2.0°$ (Fig. 6). This direction is more close to the direction expected for a geocentric axial dipole field at the sampling site (Decl = 0°; Incl = 59.4°) than to the local direction of the earth magnetic field at the date of sampling (Decl = 2.6°;

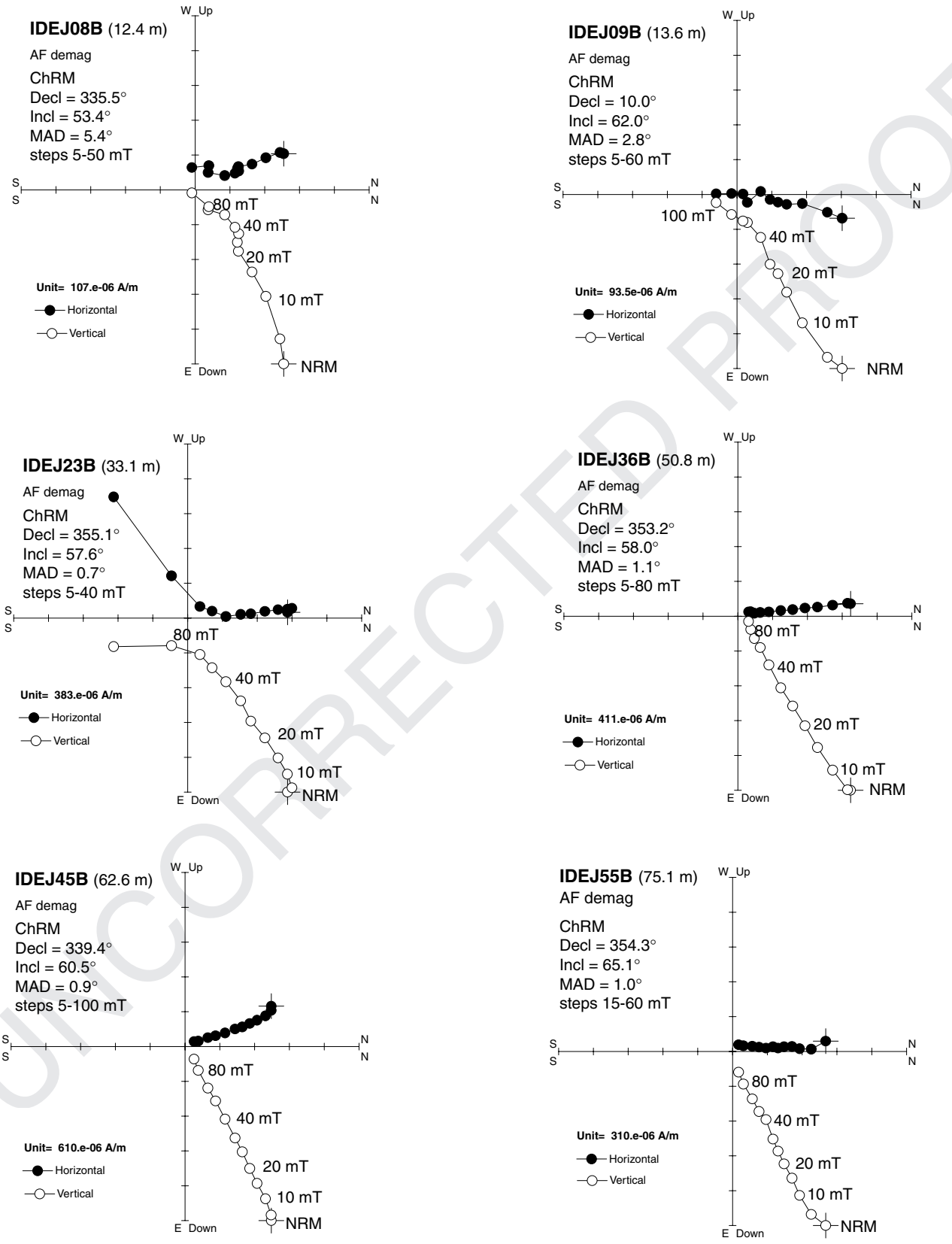

Figure 4. Representative demagnetization plots for selected specimens subjected to AF demagnetization. Orthogonal vector diagrams: open and closed symbols represent projections onto vertical and horizontal planes, respectively. The demagnetization data have been visualized and analyzed using the Remasoft program (Chadima & Hrouda 2006).

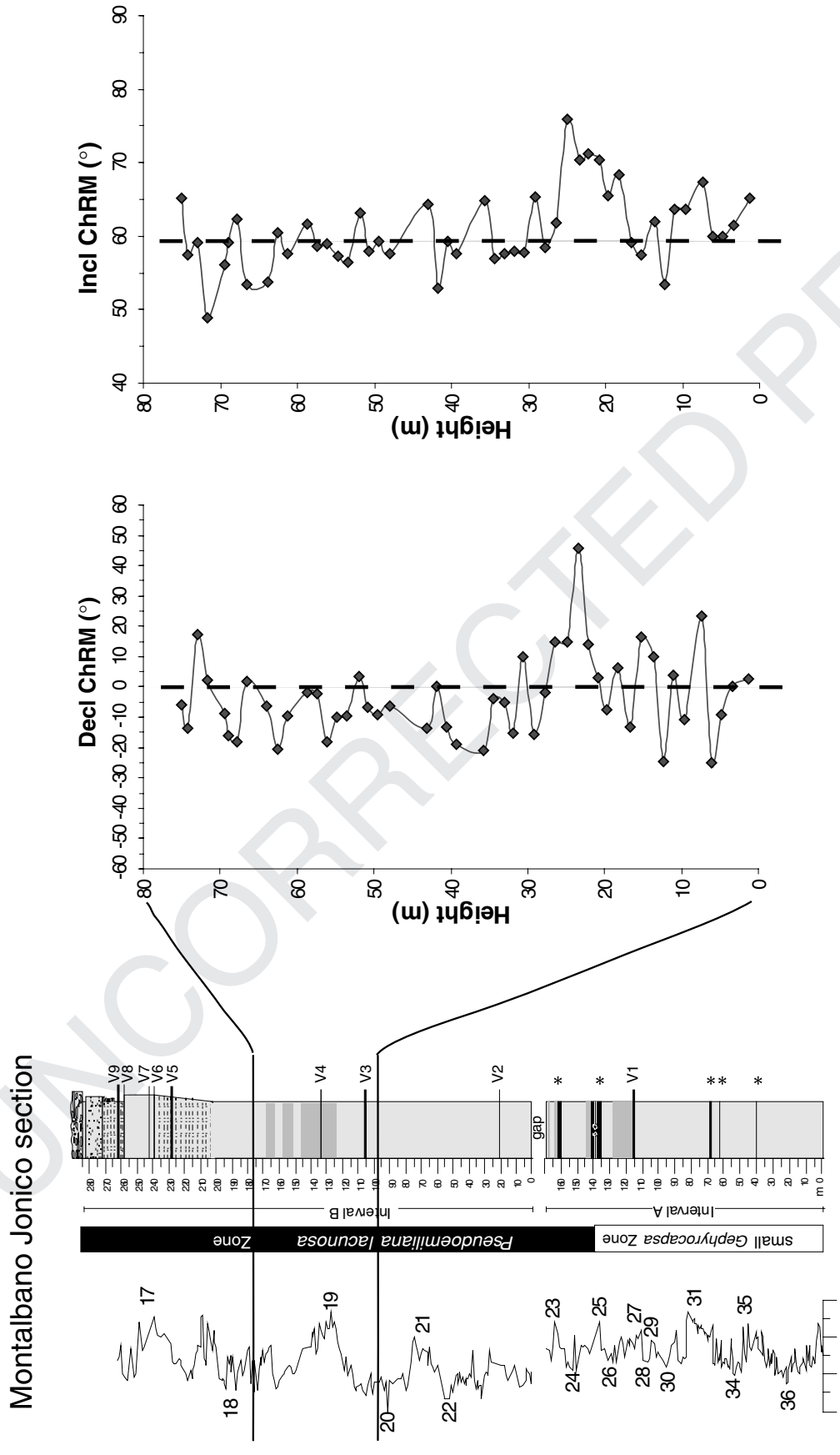

Figure 5. Stratigraphic trend of the ChRM declination and inclination for the samples of the Ideale section. The dashed lines indicate the declination and the inclination expected at the site latitude for a geocentric axial dipolar field (see text).

Table 1. Palaeomagnetic data of the Ideale section.

Specimen code	Stratigraphic height (m)	ChRM Decl (°)	ChRM Incl (°)	MAD (°)
IDEJ01C	1.3	2.5	65.2	1.3
IDEJ02B	3.3	0.1	61.5	1.6
IDEJ03B	4.5	350.8	59.9	1.6
IDEJ04C	6.1	335	60	2.5
IDEJ05B	7.4	23.5	67.4	4.7
IDEJ06B	9.6	349.4	63.7	4.2
IDEJ07B	11.0	4	63.7	5
IDEJ08B	12.4	335.5	53.4	5.4
IDEJ09B	13.6	10	62	2.8
IDEJ10C	15.3	16.5	57.4	2.9
IDEJ11B	16.6	346.8	59.2	2.3
IDEJ12B	18.2	6.2	68.3	2.3
IDEJ13A	19.7	352.6	65.5	1.9
IDEJ14B	20.8	3.2	70.4	1.7
IDEJ15B	22.2	14.2	71.2	5.3
IDEJ16B	23.4	45.9	70.3	3.6
IDEJ17B	24.9	14.8	75.9	4.2
IDEJ18B	26.4	14.9	61.8	0.8
IDEJ19B	27.8	358.3	58.4	1.6
IDEJ20B	29.2	344.2	65.3	3.7
IDEJ21	30.6	9.8	57.8	0.8
IDEJ22B	31.9	344.9	57.9	2.2
IDEJ23B	33.1	355.1	57.6	0.7
IDEJ24B	34.4	356.3	57	1.5
IDEJ25B	35.7	339.2	64.9	3.5
IDEJ27B	39.3	340.9	57.7	1.7
IDEJ28bB	40.5	346.7	59.3	3.3
IDEJ29B	41.8	0.2	52.9	2
IDEJ30B	43.1	346.2	64.4	3.7
IDEJ34	48.0	353.5	57.6	1.7
IDEJ35B	49.5	350.7	59.3	1.2
IDEJ36B	50.8	353.2	58	1.1
IDEJ37	51.9	3.5	63.2	0.8
IDEJ38C	53.5	350.6	56.4	1.3
IDEJ39C	54.8	350	57.3	1.3
IDEJ40B	56.1	341.9	59	0.4
IDEJ41B	57.4	357.6	58.6	0.7
IDEJ42B	58.7	358.2	61.7	1.8
IDEJ44B	61.3	350.3	57.7	1.3
IDEJ45B	62.6	339.4	60.5	0.9
IDEJ46C	63.9	353.5	53.8	1.6
IDEJ48A	66.5	1.7	53.5	0.5
IDEJ49B	67.8	341.9	62.3	0.7
IDEJ50A	68.9	344	59.1	2.6
IDEJ51B	69.4	351.1	56.1	0.9
IDEJ52	71.7	2.2	48.9	1.9
IDEJ53C	73.0	17.4	59.2	1.7
IDEJ54	74.3	346.4	57.4	2.4
IDEJ55B	75.1	354.3	65.1	1

Characteristic Remanence Magnetization (ChRM) isolated in the specimens subject to AF demagnetization. Decl: declination; Incl: inclination; MAD: maximum angular deviation.

Incl = 56.2° in 2008 February). The palaeomagnetic data distribution does not show inclination flattening and is characterized by a scatter $S = 10.6°$, as measured by the dispersion of the virtual geomagnetic poles and calculated according to the method of Vandamme (1994), with lower and upper error bounds of Sl = 9.1° and Su = 12.3°, respectively. This range of values is significantly lower than the S value expected at the site latitude (40°17′N), due to the palaeosecular variation of the earth magnetic field, according to both the TK03 geomagnetic field model of Tauxe & Kent (2004)

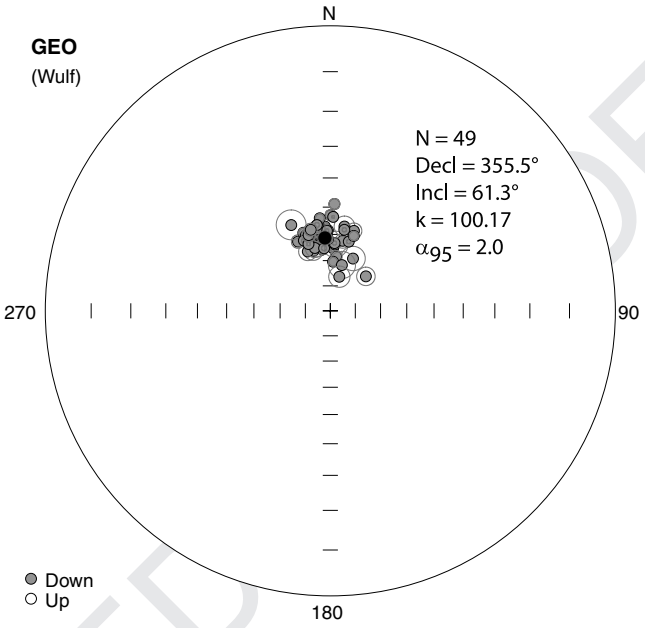

Figure 6. Equal area projection diagram of the ChRM directions isolated for the AF demagnetized specimens of the Ideale section (from 49 distinct stratigraphic levels). The circles around the ChRM directions are the maximum angular deviation and provide a quantitative measure of the precision with which each direction is determined. The data are clustered around the present-day direction of the earth magnetic field and consistently indicate a normal magnetic polarity. This result indicates that the section has been remagnetized during the Brunhes Chron. The black dot represents the section palaeomagnetic mean direction.

(which indicate a trimmed estimate of $S = 16.2°$, with error bounds of Sl = 16.1° and Su = 16.4°) and the recent global compilation of palaeomagnetic data from lava flows of Johnson *et al.* (2008) (which indicate a S mean value of 16°, almost independent from latitude for the whole Brunhes Chron).

As a further check for the obtained palaeomagnetic results, and with the aim to identify the presence of reverse magnetic polarity intervals in the MJ composite section we then collected 27 additional hand samples distributed at various lower stratigraphic intervals down to the bottom of the exposed MJ section (subsections DF-DFJ, VBJ, 5a and FG, as shown in Fig. 1), spanning an estimated age from 810 to 1240 kyrs, according to the age model of Ciaranfi *et al.* (2008, 2009). These samples are obviously expected to have a reverse polarity (Figs 1 and 2). They were not azimuthally oriented (i.e. only the vertical up and down was marked on them) and were subjected to the same demagnetization treatment as the specimens collected by *in situ* drilling during the first campaign. The obtained palaeomagnetic data showed that all the samples are characterized by a normal polarity (i.e. by a downward inclination of the ChRM) and often show a significant GRM acquisition in fields higher than 50–60 mT (Fig. 7).

Rock magnetism

The average mean magnetic susceptibility κ is of ca 200×10^{-6} SI, which is typical for clays with a low content of ferromagnetic (*sensu lato*) minerals, whose susceptibility and magnetic fabric are controlled by the paramagnetic phyllosilicates of the clay matrix (Rochette 1987; Sagnotti *et al.* 1998). The AMS data indicate that the Ideale section is characterized by a normal magnetic fabric, with

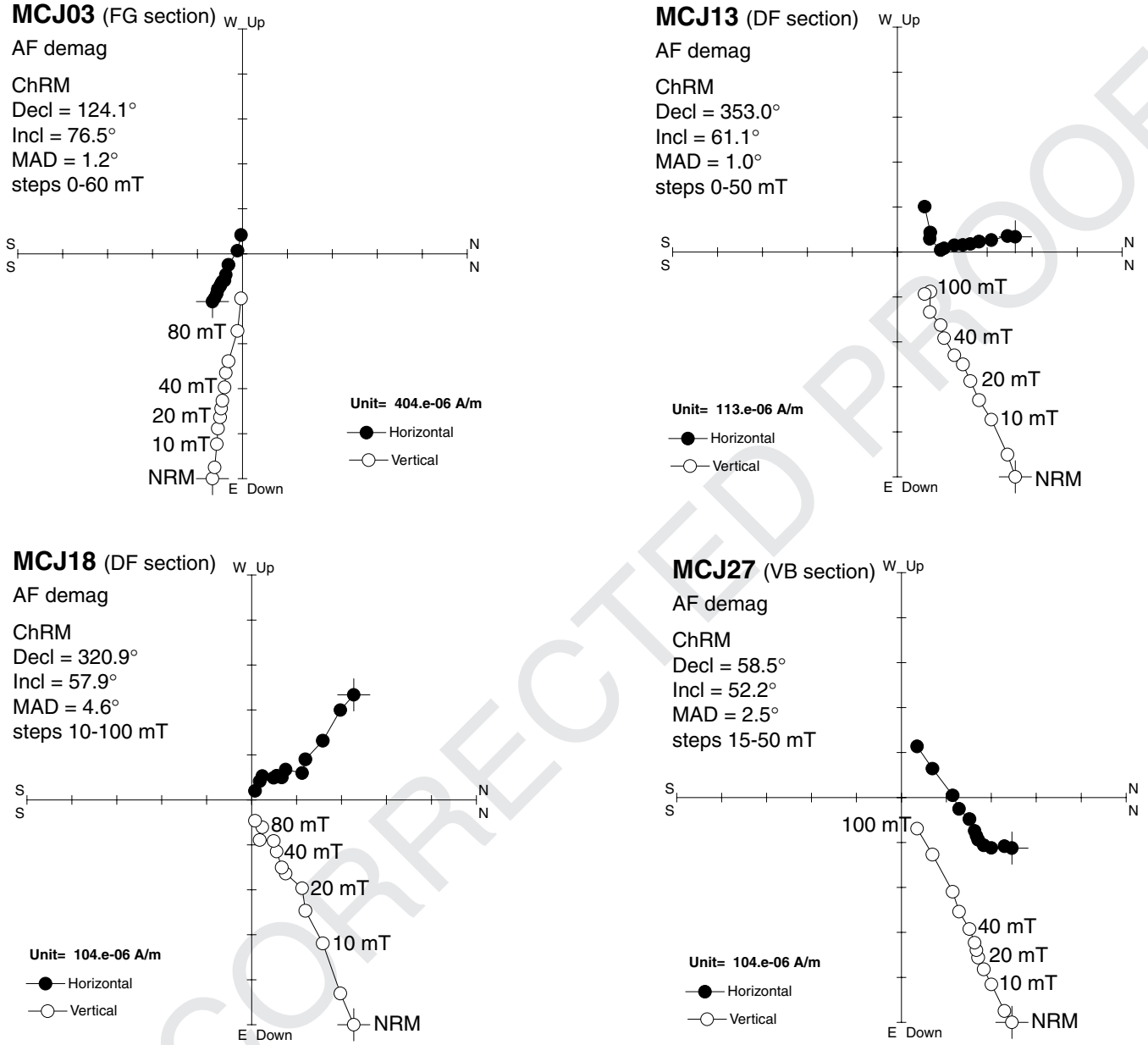

Figure 7. Representative AF demagnetization plots for selected not-azimuthally oriented hand samples collected from various intervals (see Fig. 1) lower than the Ideale section throughout the MJ composite section. Codes of the partial sections as in Fig. 1. Orthogonal vector diagrams: open and closed symbols represent projections onto vertical and horizontal planes, respectively. The demagnetization data have been visualized and analyzed using the Remasoft program (Chadima & Hrouda 2006). The data indicate that all the samples are of normal polarity.

an oblate susceptibility ellipsoid showing the minimum susceptibility axis subvertical and perpendicular to the bedding plane and a ESE–WSW oriented magnetic lineation defined by the clustering of the maximum susceptibility axes in the bedding plane (Fig. 8). The IRM acquisition curves are similar for all the samples and indicate that the IRM saturation is reached in fields of *ca*. 0.5 T (Fig. 9). The thermal demagnetization of a composite IRM shows that most of the remanence is carried by low- and intermediate-coercivity minerals (Fig. 10). For all samples the maximum unblocking temperature of the dominant IRM carrier is in the range of 300–400 °C. Only a small fraction of the IRM is left on the low-coercivity axis at temperature higher than 400 °C and it completely disappears between 500 and 600°C (Fig. 10). As a whole, the IRM data indicate that in the Ideale section the main magnetic minerals consist of an intermediate-coercivity phase with maximum unblocking temperature of 300–400 °C. The observed IRM unblocking in the temperature range between 300 and 400 °C suggests that the main magnetic mineral may be greigite (Fe_3S_4), a ferrimagnetic iron sulphide common in clays of the Italian peninsula (Sagnotti & Winkler 1999), which forms as a precursor to pyrite (FeS_2) in anoxic environment (e.g. Berner 1984; Benning *et al.* 2000; Hunger & Benning 2007) and undergoes chemical decomposition in this range of temperature (e.g. Roberts 1995; Torii *et al.* 1996; Chang *et al.* 2008). This interpretation however is not unique, since a such a decrease between 300 and 400 °C of the intermediate-coercivity IRM component could also be due to the presence of monoclinic pyrrhotite (Fe_7S_8), with a Curie temperature of *ca*. 320 °C, or to the thermochemical inversion of maghemite (γ-Fe_2O_3) to hematite (α-Fe_2O_3)

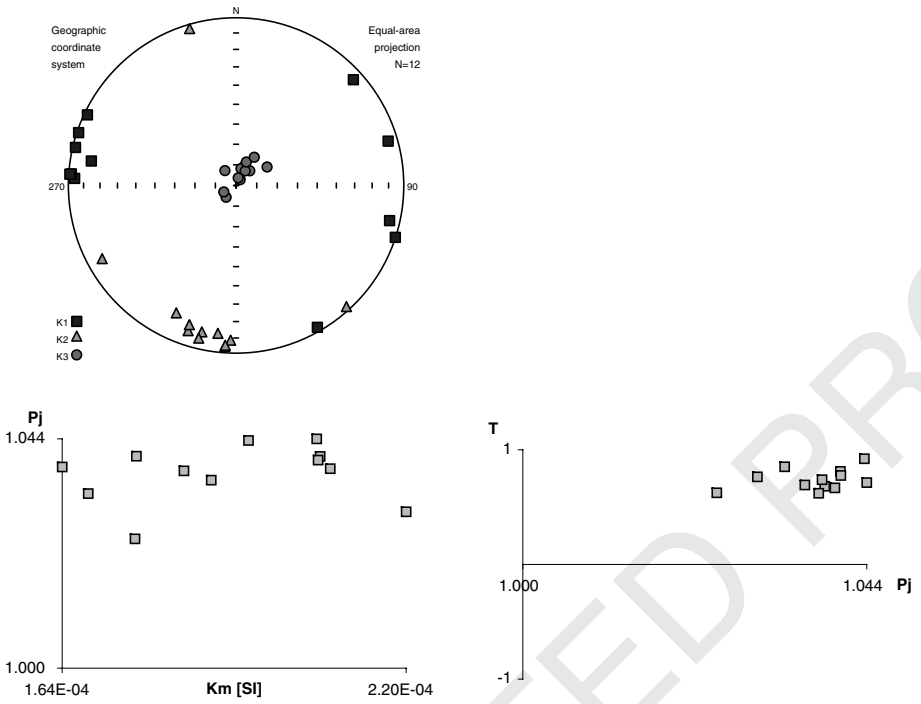

Figure 8. Anisotropy of magnetic susceptibility data for 12 samples distributed throughout the Ideale section. The data indicate a normal sedimentary-compactional fabric with oblate susceptibility ellipsoid and the minimum susceptibility axis (K3) subperpendicular to the bedding plane: K1, maximum susceptibility axis; K2, intermediate susceptibility axis; P_J, degree of anisotropy; Km, mean susceptibility; T, shape factor (Jelínek 1981).

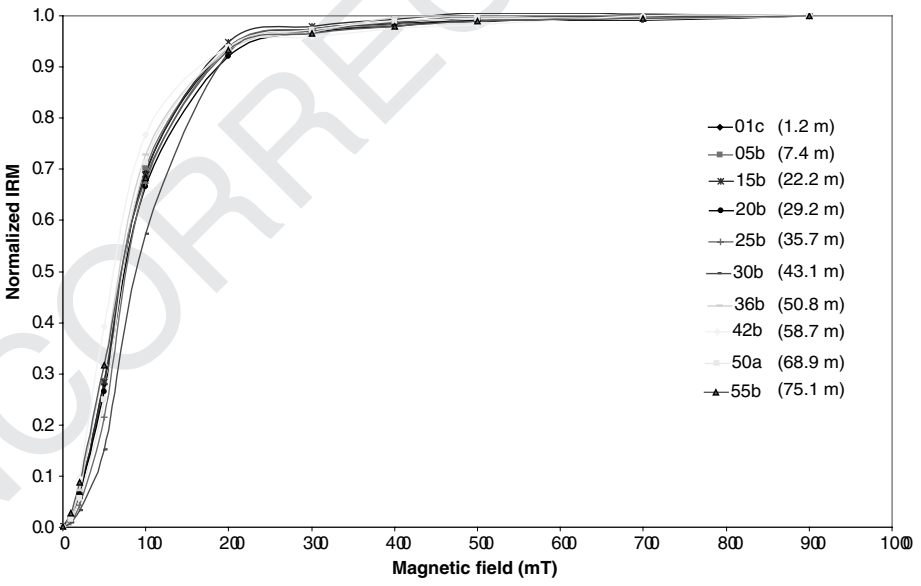

Figure 9. Stepwise acquisition of an isothermal remanent magnetization (IRM) in fields up to 1 T. The data indicate that samples saturate in a field of 0.5 T.

during heating (e.g. Dunlop & Ozdemir 1997). The IRM left at $T > 400$ °C is mostly held by the low-coercivity component and is completely demagnetized at thermal heating steps of 550–660 °C. This unambiguously indicates that magnetite (Fe_3O_4) is also present in the Ideale samples. Moreover, the acquisition of a GRM during AF demagnetization of the NRM is also a characteristic feature of greigite-bearing sediments (Snowball 1997a,b; Sagnotti & Winkler 1999; Stephenson & Snowball 2001) and the observed magnetic mineralogy alteration during thermal magnetization with production of new highly magnetic minerals at $T > 300$–350 °C is compatible with the thermal breakdown of paramagnetic pyrite, which oxidises to magnetite during heating in air (Krs *et al.* 1992; Passier *et al.* 2001).

Hysteresis data show that the magnetic behaviour is dominated by the clay matrix, with a prevailing paramagnetic slope (Fig. 11). Hysteresis loops are visible only after subtraction of the paramagnetic contribution and significant magnification close to the origin of the diagrams. Hysteresis loops are typical of small (single domain, SD and pseudo single domain, PSD) ferrimagnets with M_{RS}/M_S ratios between 0.14 and 0.57. Coercivities are definitely higher than those

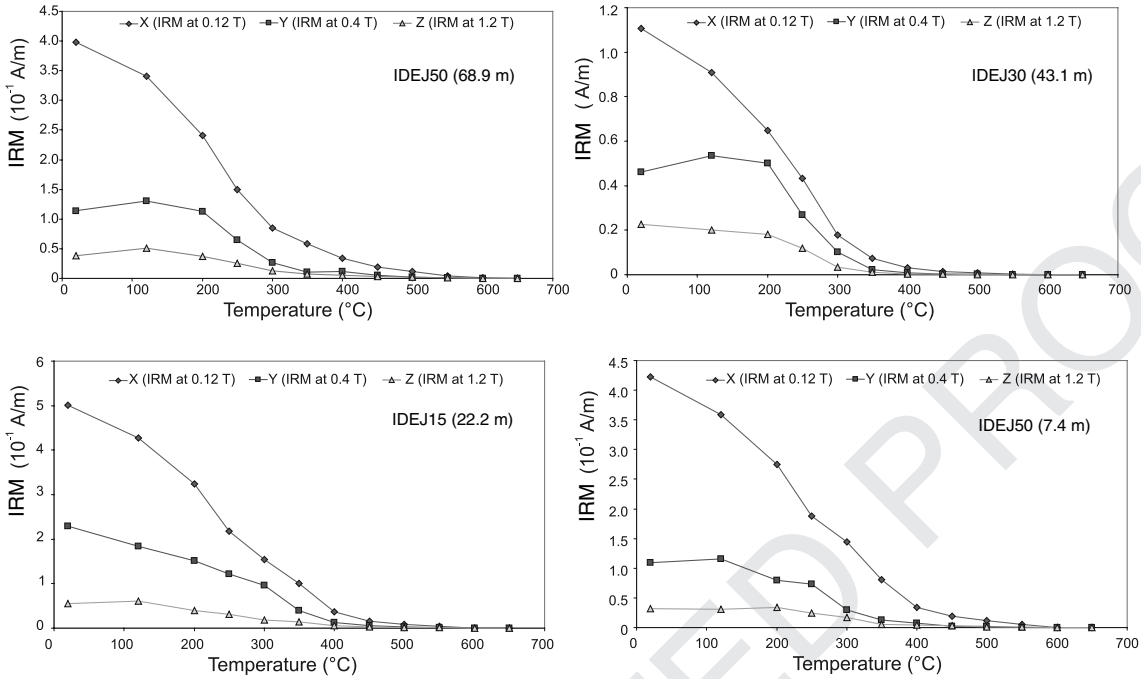

Figure 10. Representative demagnetization plots showing the data of the thermal demagnetization of a composite IRM produced in fields of 1.2, 0.4 and 0.12 T sequentially applied along the three orthogonal axes of a standard palaeomagnetic cylindrical specimen. The data indicate that most of the IRM is carried by soft- and intermediate-coercivity components (*X* and *Y* axes), with maximum unblocking temperatures mainly in the range 350–400 °C and subordinately in the range 500–550 °C.

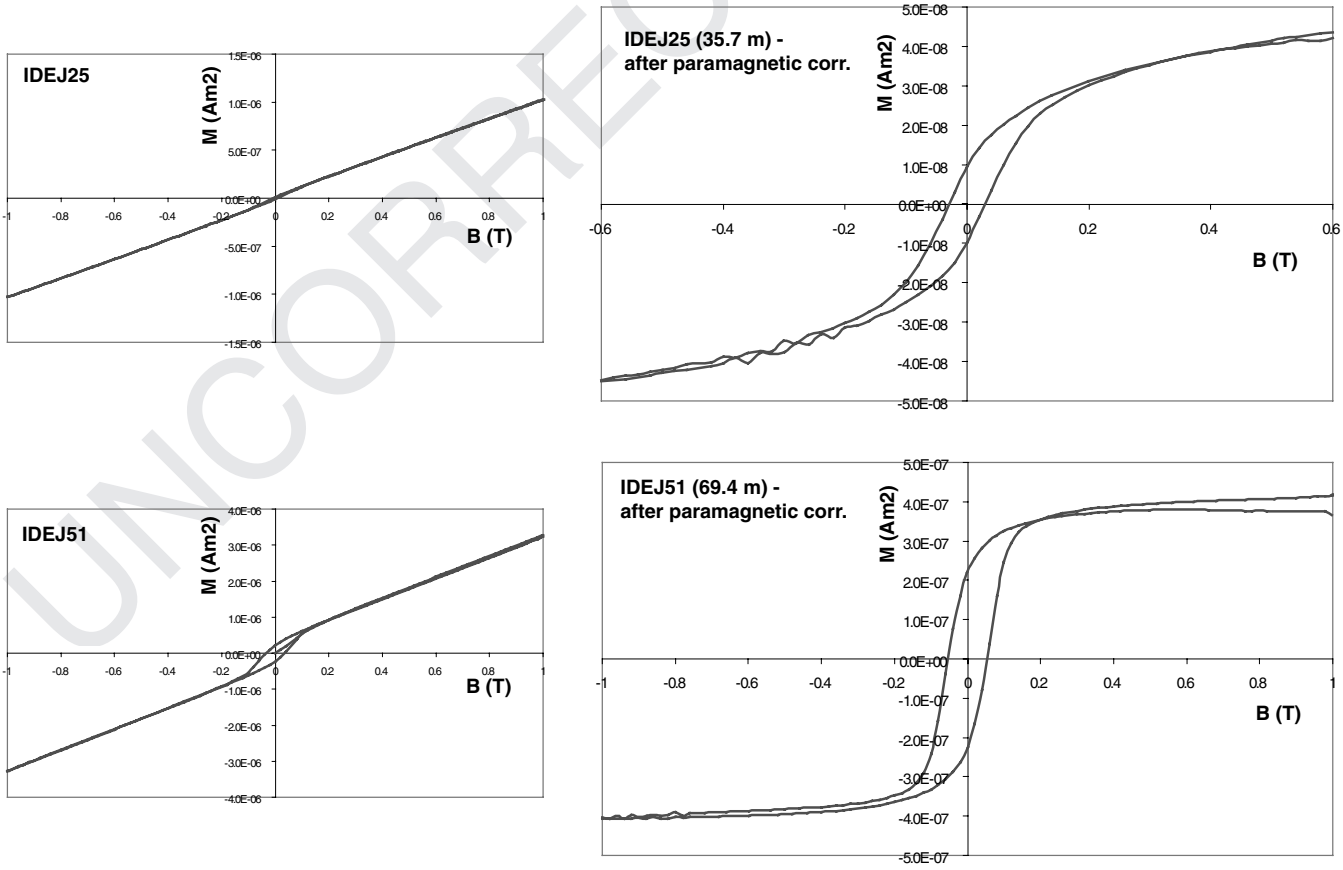

Figure 11. Two representative hysteresis cycles for the samples of the Ideal section. B: magnetic induction; M: magnetic moment. The data indicate the strong paramagnetic contribution of the clay matrix (left-hand diagrams). Hysteresis loops are evident only after a substantial magnification close to the origin (right-hand diagrams). The hysteresis loops are typical of fine ferromagnetic grains (SD and PSD).

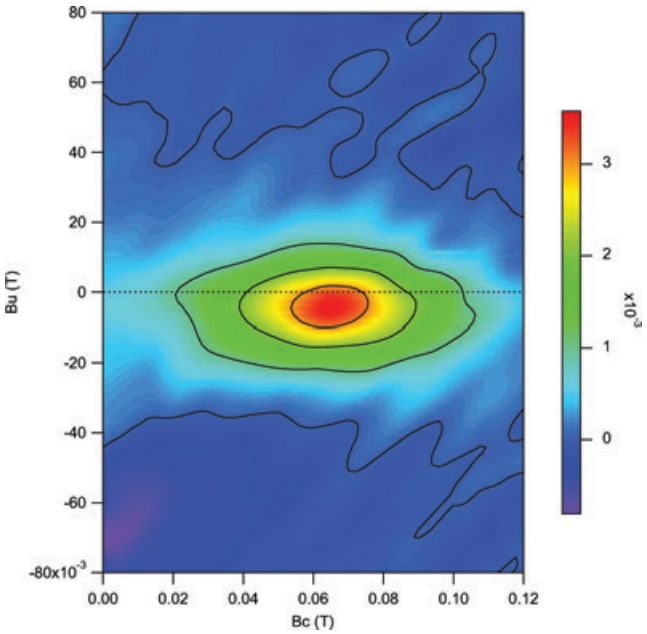

Figure 12. A representative FORC diagram, obtained for the sample with the highest magnetization (IDEJ51, at 69.4 m in the Ideale section). The diagram shows closed concentric contours lines about a central peak, which is typical for SD grains. The value of Bc at the peak of the distribution is ca. 65 mT, which is typical for greigite. The vertical spread in the Bu direction of this FORC distribution is a manifestation of magnetic interaction, as well as the offset of the FORC distribution below the Bu = 0 axis.

typical for magnetite; B_{CR} varies in the range 60–70 mT and B_C between 25 and 54 mT, which fit the ranges of values reported for greigite (Roberts 1995; Sagnotti & Winkler 1999; Roberts *et al.* 2006).

FORC diagrams are characterized by closed concentric contours about a central peak and have a negative region in the lower left-hand part of the diagram (Fig. 12). The coercivity distribution, the value of B_C at the peak of the distribution (60–70 mT) and the negative region in the lower left-hand part of the diagram are typical for SD greigite grains (Roberts *et al.* 2006). A significant degree of magnetic interaction between the magnetic grains is also suggested by the vertical spread in the B_U direction and by the offset of the FORC distribution below the $B_U = 0$ axis (Roberts *et al.* 2000, 2006).

As a whole, the rock magnetism data suggest that greigite is the main magnetic mineral in the studied samples.

FE-SEM observations and analyses

Iron sulphide minerals can be easily identified under FE-SEM due to their high electron backscatter and obvious microtextures. Iron sulphides occur mostly as euhedral crystals either isolated and dispersed within the clay matrix or in closely packed aggregates filling sediment voids (Fig. 13). The composition of iron sulphide grains has been determined by acquiring EDS X-ray spectra (Fig. 14). Beam interaction volume and analysed grains being of similar size, some matrix contamination appears in the spectra as peaks from oxygen, silica, and other elements from clay minerals. However, the ratio between Fe and *S* allows to clearly distinguish pyrite [33 per cent (at. per cent)Fe; 67 per cent S] from greigite (43 per cent Fe; 57 per cent S). Most of the analyzed iron sulphide grains consist of pyrite, which is paramagnetic. The framboidal aggregation (a framboid is a spherical aggregate of equigranular microcrystals, e.g. Schallreuter 1984), which represents the typical morphology for pyrite occurrence in sediments, was not observed for pyrite crystals in the analyzed samples. The lack of framboids may indicate no early diagenetic growth of iron sulphides in these sediments. In fact, framboids are usually the earliest phase in samples with multiple generations of sulphide growth (Raiswell 1982). In our samples, greigite usually occurs as grains of smaller size (submicron) with respect to pyrite, which could explain the higher contamination of clay elements observed in the EDS X-ray spectra of the former (Fig. 14). Greigite grains also show a darker contrast with respect to pyrite (Figs 13a and c), probably due to their less regular surfaces (Roberts & Weaver 2005). A grain size in the micron to submicron range is compatible with the SD–PSD magnetic state suggested by the hysteresis properties. As for pyrite, greigite mostly occurs both as individual euhedral crystals (Fig. 13f) dispersed within the clay matrix and as closely packed aggregates of cubo-octahedra crystals with uniform equi-granular submicron size within iron-sulphide fillings that are surrounded by the clay matrix (Figs 13a–f). Occasionally, greigite was also found in spherical to subspherical framboidal aggregates (Fig. 13d). No magnetite grains were found at the FE-SEM observations and analyses.

DISCUSSION AND CONCLUSIONS

Given the consistency of all the stratigraphic constraints, the Ideale section was expected to span across the Brunhes-Matutayama reversal boundary. Instead, the obtained palaeomagnetic results showed a constant normal polarity throughout the Ideale section and indicate that the whole exposed composite MJ section has been remagnetized by a pervasive greigite growth during the Brunhes Chron (i.e. in the last 780 ka). The absence of an inclination flattening is consistent with the hypothesis of a diagenetically formed greigite (see Vasiliev *et al.* 2008). The relatively low scatter of the palaeomagnetic data, with respect to the dispersion expected for the geomagnetic secular variation at the site latitude, suggests that the data do not represent a long time interval and that the remagnetization occurred in a single short period.

Greigite generally forms authigenetically in anoxic sedimentary environments as an intermediate product in the chemical pathway to pyrite formation (Berner 1970, 1984). It has been earlier reported in the Pleistocene clays of the Montemesola basin in the Apulian Foreland (Ciaranfi *et al.* 1971; Garavelli & Nuovo 1971), also belonging to the 'argille subappennine' unit of southern peninsular Italy, and interpreted as an early diagenetic product formed by reductive processes associated with the bacterial decomposition of organic matter. Since then greigite has been recognized in several other clays of the Italian peninsula (Sagnotti & Winkler 1999) and its widespread occurrence in rapidly deposited fine-grained marine sediments is now well established world wide (Rowan *et al.* 2009). In standard diagenetic zonation models, the nucleation and growth of greigite grains occurs in the earliest stages of diagenesis, just below the water-sediment interface, in association with bacterially mediated chemical reactions driven by the degradation of organic matter and involving the reduction of sulphate and the dissolution of ferric iron-bearing minerals (Berner 1970, 1984; Wilkin & Barnes 1997; Benning *et al.* 2000). In the chemical reaction pathway to pyrite, the intermediate products (precursor phases) iron monosulphide, mackinawite and greigite are thermodynamically unstable relative to pyrite (Berner 1967) and rates of pyritization may be very fast

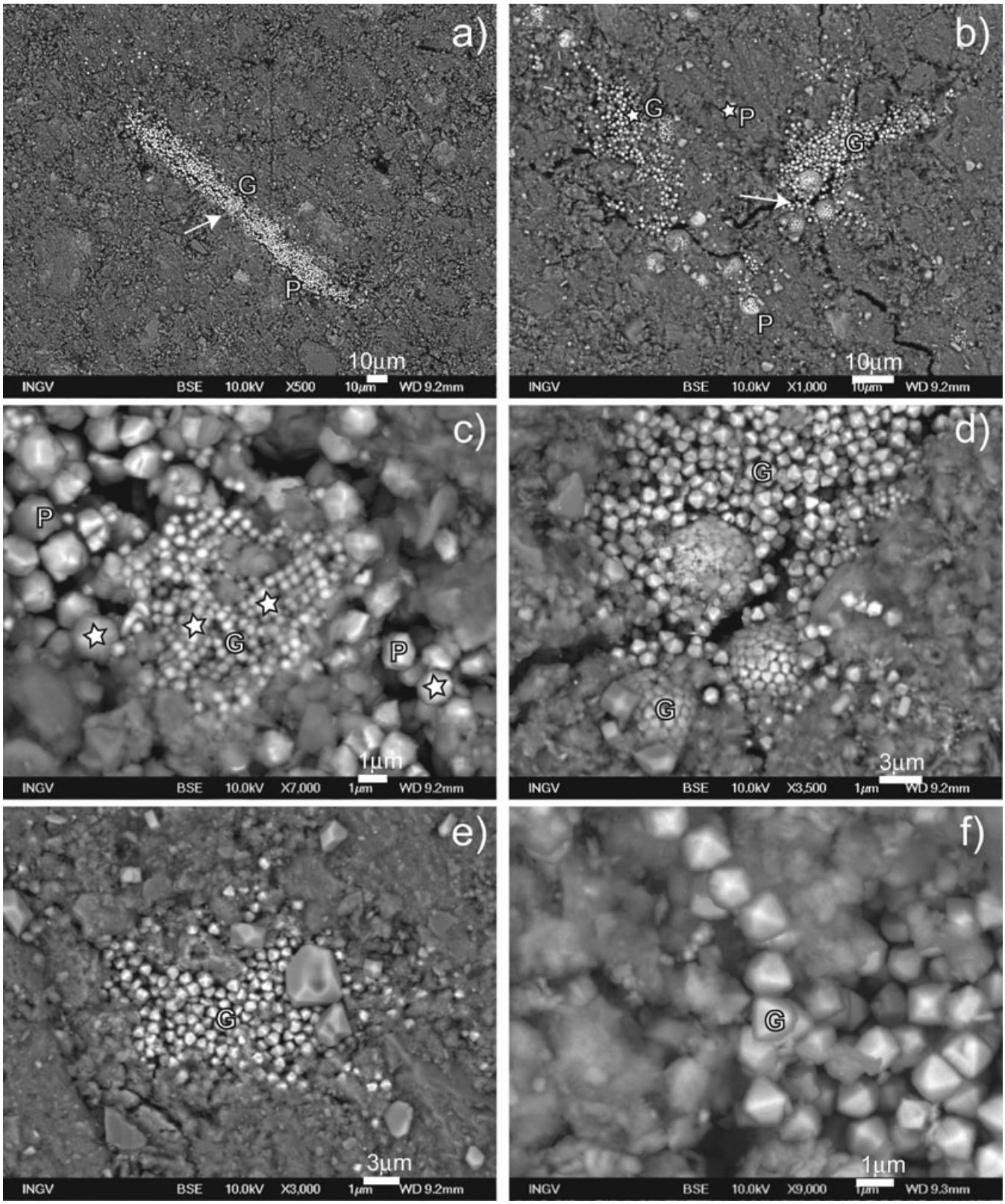

Figure 13. Representative FE-SEM images of sample IDEJ30 (taken at 43.1 m in the Ideale section). Low-magnification images show iron sulphides (bright tones) both dispersed throughout the matrix and filling elongate (a) or irregular (b) areas. Stars mark the location of some of the EDS analyses reported in Fig. 14. (c) Enlargement of the central area of (a) (marked by arrow), showing a cluster of submicron sized greigite (G) crystals surrounded by larger euhedral pyrite (P) ones. (d) Enlargement of part of (b) (marked by arrow) showing greigite crystals in subspherical framboidal aggregates. (e) Irregular greigite aggregate. (f) Detail of octahedral greigite crystals.

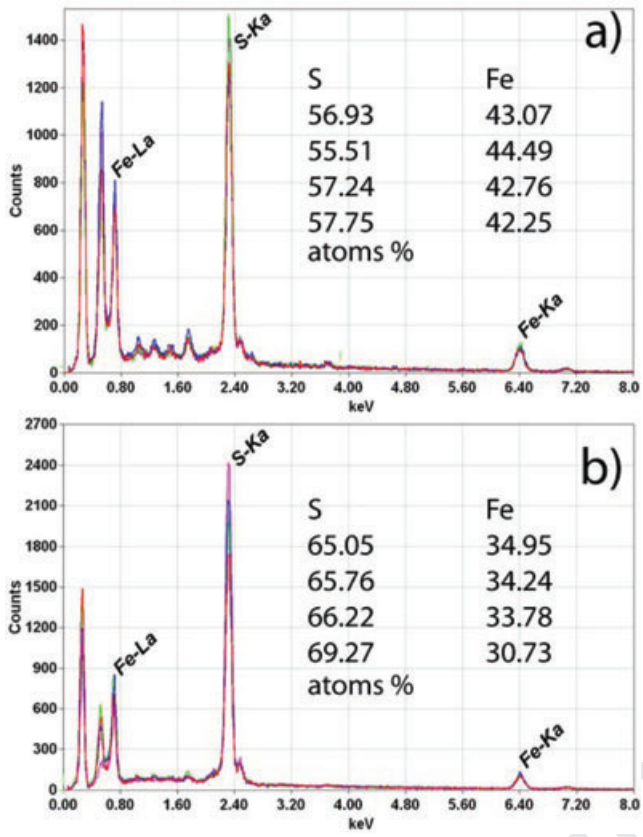

Figure 14. Eight EDS X-ray spectra showing the main emission lines and the correspondent atomic abundances, as derived from standardless chemical analyses, of Fe and S in greigite (a) and pyrite (b) crystals.

(geologically instantaneous), with characteristic timescales of the order of hours to days (Wilkin & Barnes 1997). However greigite can be, at least partially, preserved in sediments if the supply of organic carbon is limited in presence of abundant reactive iron (Kao *et al.* 2004). Syn-sedimentary greigite may also be produced biogenically, in forms of magnetosomes, by magnetotactic bacteria (Farina *et al.* 1990; Mann *et al.* 1990; Bazylinski *et al.* 1993; Vasiliev *et al.* 2008). In the cases of a biogenic or early diagenetic formation greigite may preserve a primary ChRM which is almost coeval with the host sediments. However, it has been well established that greigite can commonly form at a late diagenetic stage in fine-grained sedimentary sequences, thus acquiring. a chemical remanent magnetization (CRM) which is significantly younger than the hosting sediments (e.g. Florindo & Sagnotti 1995; Thompson & Cameron 1995; Horng *et al.* 1998; Richter *et al.* 1998; Jiang *et al.* 2001; Sagnotti *et al.* 2005; Rowan & Roberts 2008; Porreca *et al.* 2009). A variety of different mechanisms for such a late diagenetic growth has been recognized. They are associated to changes in the pore water chemistry which disrupt the steady-state diagenetic progression. Such mechanisms are linked to the migration of mineralized fluids which may result from a variety of forcing events, such as anaerobic oxidation of methane in cold seeps, (e.g. from underlying organic-rich sapropels), gas hydrate migration, tectonic events, convection of seawater in the vicinity of mud volcanoes, migration of sulphate from deep geological reservoirs such as evaporitic deposits, large amplitude sea level change in continental shelves and cyclic variation of bottom water oxygenation and submarine landslides (e.g. Roberts & Weaver 2005 and references therein). In all these cases, the late diagenetic growth of greigite grains leads to a widespread remagnetization of the host sediments that compromises magnetostratigraphic studies in greigite-bearing sedimentary sequences. A variety of syndepositional, early diagenetic and late diagenetic growth of greigite has been reported for fine-grained sediments of different ages in the Italian peninsula on the basis of various palaeomagnetic and stratigraphic constraints (Table 2). In the MJ section the normal magnetic polarity acquired during the Brunhes Chron (i.e. less than 780 ka ago) extends down to the lowermost exposed interval, which has an astronomically calibrated age of 1240 ka. This observation provides evidences for a delay in greigite formation of at least the order of half million years, which is the longest documented so far in Italy.

The AMS ellipsoid reconstructed for the Ideale section indicates a magnetic fabric typical of clayey sediments at the earliest stages of deformation, where the magnetic foliation corresponds to the bedding-compaction plane and the magnetic lineation may indicate the local direction of the maximum elongation strain (Mattei *et al.* 1997). In apparently 'undeformed' clays such magnetic lineation may arise as an intersection lineation of differently oriented basal planes of the clay minerals (e.g. chlorite), reflecting the orientation of their common axes (Cifelli *et al.* 2004, 2005). Given the relatively low value of the magnetic susceptibility and the low concentration of ferromagnetic minerals in the MJ sequence it is not possible to reconstruct the preferred orientation of the magnetic carriers (e.g. greigite grains) by means of AMS analyses.

In this study, the modes of occurrence of the main magnetic minerals, has been reconstructed by direct observation with the FE-SEM. The recognition of euhedral greigite crystals, either as isolated grains dispersed in the clay matrix or as closely packed aggregates filling sediment voids, suggests that the studied sediments have been subjected either to a prolonged early diagenetic sulphidization event resulting from evolving pore water compositions or to more than one sulphidization events, the latter being caused by migration of fluids during the Brunhes Chron. The fact that all microcrystals within any one aggregate have the same size and morphology suggests that the microcrystals nucleate simultaneously and grow at the same rate for the same time prior to aggregation (Wilkin & Barnes 1997). The simple texture of the sulphide aggregates and the limited occurrence of the framboids suggests that that late sulphide growth is volumetrically much more significant than early growth. The remagnetization of the entire exposed MJ composite section and the estimated delay in CRM acquisition (at least 450 ka) implies a widespread late diagenetic sulphidization event associated with the greigite growth. We speculate that the sulphidization events also induced the dissolution of the primary detrital magnetic oxides originally present in the sedimentary sequence.

The present results indicate that the MJ section does not fulfil the guiding primary criterion of the GSSP of Ionian Stage due to its unreliable magnetostratigraphic record. However, the excellent land exposure of the section, its stratigraphic continuity, the numerous chronological constraints and the astronomical calibration indicate that the section is an essential reference record for the Lower–Middle Pleistocene.

ACKNOWLEDGMENTS

We are grateful to Prof Leonardo Giordano, major of Montalbano Jonico and to Drs Luciano and Gianclemente Miraglia for their support and help with sampling and with the logistics in the field. This study was financially supported by 'Fondi Ateneo' 2007 (University of Bari) granted to R. La Perna. We thank Chris Rowan and Silja Hüsing for their constructive reviews, and the Editor Cor

Table 2. Timing of greigite formation in Italian clays.

Locality	Age	Timing	Constraints	Estimated delay
Valle Ricca[a]	Upper Pliocene	Late diagenetic	Wrong polarity	> 150 kyr
Pian del Gaudo basin[b]	Middle Pleistocene	Late diagenetic	Fold test	> ~300 kyr
Montalbano Jonico[c]	Middle Pleistocene	Late diagenetic	Wrong polarity, SEM observations	Unknown (>450 kyr ?)
Sant'Arcangelo basin[d]	Upper Pliocene- Lower Pleistocene	Early diagenetic	Fold test, polarity	- (delays of a few kry not resolvable)
Amantea basin[e]	Tortonian-Messinian	Early diagenetic	Fold test, polarity	- (delays of a few kry not resolvable)
External northern Apennines[f]	Tortonian-Messinian	Early diagenetic	Fold test, polarity	- (delays of a few kry not resolvable)
External central Apennines[g]	Plio-Pleistocene	Both late and early diagenetic	Mixed evidences	Unknown (variable)
Crostolo River[h]	Plio-Pleistocene (Upper Olduvai)	Both late and early diagenetic	Mixed evidences	Unknown (variable)
Monte dei Corvi Beach section[i]	Middle-Upper Miocene	Early diagenetic	Polarity	<5–10 kry

Notes: [a]Florindo & Sagnotti (1995), [b]Porreca *et al.* (2009), [c]this study, [d]Sagnotti (1992), [e]Speranza *et al.* (2000), [f]Speranza *et al.* (1997); [g]Sagnotti *et al.* (2000), [h]Roberts *et al.* (2005), [i]Hüsing *et al.* (2009).

Langereis for his suggestions and help with the data analysis. All their comments allowed to significantly improve the manuscript.

REFERENCES

Azzaroli, A., 1968. Studi illustrativi della carta geologica d'Italia–Formazioni geologiche, *Servizio Geologico d'Italia,* **I,** 183–185.

Bazylinski, D.A., Heywood, B.R., Mann, S. & Frankel, R.B., 1993. Fe_3O_4 and Fe_3S_4 in a bacterium, *Nature,* **366,** 218.

Benning, L.G., Wilkin, R.T. & Barnes H.L., 2000. Reaction pathways in the Fe–S system below 100 8C, *Chem. Geol.,* **167,** 25– 51.

Berner, R.A., 1967. Thermodynamic stability of sedimentary iron sulfides, *Am. J. Sci.,* **265,** 773–785.

Berner, R.A., 1970. Sedimentary pyrite formation, *Am. J. Sci.,* **268,** 1–23.

Berner, R.A., 1984. Sedimentary pyrite formation: an update, *Geoch. Cosmochem. Acta.,* **48,** 605–615.

Bickert, T., Curry, W.B. & Wefer, G., 1997. Late Pliocene to Holocene (2.6–0 Ma) western equatorial Atlantic deep-water circulation: inferences from benthic stable isotope, in *Proceedings of the Ocean Drilling Program, Scientific Results,* Vol. 154, pp. 239–253, eds Shackleton, N.J., Curry, W.B., Richter, C. & Bralower, T.J., College Station (TX). Q4

Brilli, M., Lerche, I., Ciaranfi, N. & Turi, B., 2000. Evidences of precession and obliquity orbital forcing in oxygen-18 isotope composition of Montalbano Jonico Section (Basilicata, southern Italy), *Appl. Radiat. Isotopes,* **52,** 957–964.

Chadima, M. & Hrouda, F., 2006. Remasoft 3.0–a user-friendly paleomagnetic data browser and analyzer, *Travaux Géophysiques,* **XXVII,** 20–21.

Chang, L., Roberts, A.P., Tang, Y., Rainford, B.D., Muxworthy, A.R. & Chen, Q., 2008. Fundamental magnetic parameters from pure synthetic greigite (Fe3S4), *J. geophys. Res.,* **113,** B06104, doi:10.1029/2007JB005502.

Channell, J.E.T., Curtis, J.H. & Flower, B.P., 2004. The Matuyama-Brunhes boundary interval (500–900 ka) in North Atlantic drift sediments, *Geophys. J. Int.,* **158,** 489–505.

Ciaranfi, N. & D'Alessandro, A., 2005. Overview of the Montalbano Jonico area and section: a proposal for a boundary stratotype for the lower–middle Pleistocene, Southern Italy Foredeep, *Quat. Int.,* **131,** 5–10.

Ciaranfi, N., Nuovo, G. & Ricchetti, G., 1971. Le argille di Taranto e di Montemesola: studio geologico, geochimica e paleontologico, *Boll. Soc. Geol. It.,* **90,** 293–314.

Ciaranfi, N., D'Alessandro, A. & Marino, M., 1997. A candidate section for the Lower-Middle Pleistocene Boundary (Apennine Foredeep, South Italy), in *Proceedings 30th International Congress,* Vol. 11, pp. 201–211, eds Naiwen, W. & Remane, J. Q5

Ciaranfi, N., D'Alessandro, A., Girone, G., Maiorano, P., Marino, M., Soldani, D. & Stefanelli, S., 2001. Pleistocene sections in the Montalbano Jonico area and the potential GSSP for Early-Middle Pleistocene in the Lucania Basin (Southern Italy), *Memorie Scienze Geologiche,* **53,** 67–83.

Ciaranfi, N. *et al*., 2008. The Lower-Middle Pleistocene Montalbano Jonico Section in the Southern Apennine Foredeep, *Geosed 2008*, Bari 23–27 settembre, 32–33, Abstracts.

Ciaranfi, N. *et al*., 2009. Integrated Stratigraphy and Astronomical Tuning of Lower-Middle Pleistocene Montalbano Jonico Land Section (Southern Italy), *Quater. Int.,* in press, doi:10.1016/j.quaint.2009.10.027. Q6

Cifelli, F., Mattei, M., Hirt, A.M. & Gunther, A., 2004. The origin of tectonic fabrics in "undeformed" clays: the early stages of deformation in extensional sedimentary basins, *Geophys. Res. Lett.,* **31,** L09604, doi:10.1029/2004GL019609.

Cifelli, F., Mattei, M., Chadima, M., Hirt, A.M. & Hansen, A., 2005. The origin of tectonic lineation in extensional basins: combined neutron texture and magnetic analyses on "undeformed" clays, *Earth planet. Sci. Lett.,* **235,** 62–78.

Cita, M.B., 2008. Summary of Italian marine stages of the Quaternary, *Episodes,* **31,** 251–254.

Cita, M.B., Capraro, L., Ciaranfi, N., Di Stefano, E., Marino, M., Rio, D., Sprovieri, R. & Vai, G.B., 2006. Calabrian and Ionian: a proposal for the definition of Mediterranean stages for Lower and Middle Pleistocene, *Episodes,* **29**(2), 107–114.

Cita, M.B. *et al*., 2008. The Calabrian Stage redefined, *Episodes,* **31**(4), 408–419.

Coe, R.S., Singer, B.S., Pringle, M.S. & Zhao, X., 2004. Matuyama–Brunhes reversal and Kamikatsura event on Maui: paleomagnetic directions, 40Ar/39Ar ages and implications, *Earth planet. Sci. Lett.,* **222,** 667–684.

Comas, M.C., Zahn, R., Klaus, A. *et al*., 1996. *Proceedings of the Ocean Drilling Program, Initial Reports,* Vol. 161. College Station, TX (Ocean Drilling Program), doi:10.2973/odp.proc.ir.161.1996.

de Kaenel, E., Siesser, W.G. & Murat, A., 1999. Pleistocene calcareous nannofossil biostratigraphy and the Western Mediterranean sapropels, Sites 974 to 977 and 979. in *Proceedings of the Ocean Drilling Program -Scientific Results,* Vol. 161, pp. 159–181, College Station, TX.

Drouin, D., Réal Couture, A., Joly, D., Tastet, X., Aimez, V. & Gauvin, R., 2007. CASINO V2.42—a fast and easy-to-use modeling tool for scanning electron microscopy and microanalysis users, *Scanning,* **29,** 92–101, doi:10.1002/sca.20000.

Dunlop, D.J. & Özdemir, Ö., 1997. *Rock Magnetism: Fundamentals and Frontiers,* 573 pp., Cambridge Univ. Press, New York.

Farina, M., Esquivel, D.M.S. & Lins de Barros, H.G.P., 1990. Magnetic iron-sulphur crystals from a magnetotactic microorganism, *Nature,* **343,** 256–258.

Fisher, R.A., 1953. Dispersion on a sphere, *Proc. Roy. Soc. Lond.,* **A217,** 295–305.

Florindo, F. & Sagnotti, L., 1995. Palaeomagnetism and rock magnetism in the upper Pliocene Valle Ricca (Rome, Italy) section, *Geophys. J. Int.,* **123,** 340–354.

Fu, Y., von Dobeneck, T., Franke, C., Heslop, D. & Kasten S., 2008. Rock magnetic identification and geochemical process models of greigite formation in Quaternary marine sediments from the Gulf of Mexico (IODP Hole U1319A), *Earth planet. Sci. Lett.,* **275,** 233–245.

Garavelli, C.L. & Nuovo, G., 1971. La greigite delle argille di Montemesola. *Periodico di Mineralogia,* **40,** 305–327.

Harrison, R.J. & Feinberg, J.M., 2008. FORCinel: An improved algorithm for calculating first-order reversal curve distributions using locally weighted regression smoothing, *Geochem. Geophys. Geosyst.,* **9,** Q05016, doi:10.1029/2008GC001987.

Horng, C.S., Torii, M., Shea, K.-S. & Kao, S.-J., 1998. Inconsistent magnetic polarities between greigite- and pyrrhotite/magnetite bearing marine sediments from the Tsailiao-chi section, southwestern Taiwan, *Earth planet. Sci. Lett.,* **164,** 467–481.

Hunger, S. & Benning, L.G., 2007. Greigite: a true intermediate on the polysulfide pathway to pyrite, *Geochem. Trans.,* **8,** doi:10.1186/1467-4866-8-1.

Hüsing, S.K., Kuiper, K.F., Link, W., Hilgen, F.J. & Krijgsman, W., 2009. The upper-Tortonian-lower Messinian at Monte dei Corvi (Northern Apennines, Italy): completing a Mediterranean reference section for the Tortonian Stage, *Earth planet. Sci. Lett.,* **282,** 140–157.

Jelínek, V., 1978. Statistical processing of anisotropy of magnetic susceptibility measured on groups of specimens. *Stud. Geophys. Geod.,* **22,** 50–62.

Jelínek, V., 1981. Characterization of the magnetic fabrics of rocks, *Tectonophysics,* **79,** 63–67.

Jiang, W.T., Horng, C.S., Roberts, A.P. & Peacor, D.R., 2001. Contradictory magnetic polarities in sediments and variable timing of neoformation of authigenic greigite, *Earth planet. Sci. Lett.,* **193,** 1–12.

Joannin, S., 2007. Changements climatiques en méditerranée à la transition Pléistocène inférieur-moyen: pollens, isotopes stables et cyclostratigraphie. *Unpubl. PhD thesis*. University Lyon 1, France.

Joannin, S., Ciaranfi, N. & Stefanelli, S., 2008. Vegetation changes during the late Early Pleistocene at Montalbano Jonico (Province of Matera, southern Italy) based on pollen analysis. *Palaeogeog. Palaeclimat. Palaeoecol.,* **270**(1–2), 92–101.

Johnson, C.L. *et al*., 2008. Recent investigations of the 0–5 Ma geomagnetic field recorded by lava flows, *Geochem. Geophys. Geosyst.,* **9,** Q04032, doi:10.1029/2007GC001696.

Kao, S.J., Horng, C.S., Liu, K.K. & Roberts, A.P., 2004. Carbon-Sulfur-Iron Relationships in Sedimentary Rocks from Southwestern Taiwan: influence of Geochemical Environment on Greigite and Pyrrhotite Formation, *Chem. Geol.,* **203,** 153–168.

Kirschvink, J.L., 1980. The least-square line and plane and the analysis of paleomagnetic data. *Geophys. J. R. astr. Soc.,* **62,** 699–718.

Krs, M., Novak, F., Krsova, M., Pruner, P., Kouklikova, L. & Jansa, J., 1992. Magnetic properties and metastability of greigite-smythite mineralization in brown-coal basins of the Krusné hory Piedmont, Bohemia, *Phys. Earth planet. Inter.,* **70,** 273–287.

Laskar, J., Robutel, P., Joutel, F., Gastineau, M., Correia, A.C.M. & Levrard, B., 2004. A longterm numerical solution for the insolation quantities of the Earth. *Astron. Astrophys.,* **428,** 261–285, doi:10.1051/0004-6361:20041335.

Lisiecki, L. & Raymo, M., 2005. A Pliocene-Pleistocene stack of 57 globally distributed benthic $\delta^{18}O$ records, *Paleoceanography,* **20**(1), doi:10.1029/2004PA001071.

Lourens, L., 2004. Revised tuning of Ocean Drilling Program Site 964 and KC01B (Mediterranean) and implications for the $\delta^{18}O$, tephra, calcareous nannofossil, and geomagnetic reversal chronologies of the past 1.1 Myr, *Paleoceanography,* **19**(3), PA3010, doi:10.1029/2003PA000997.

Lourens, L., Hilgen, F., Shackleton, N.J., Laskar, J. & Wilson, D., 2004. The Neogene Period, in *A Geological Time Scale* pp. 409–440, eds Gradstein, F.M., Ogg, J.G. & Smith, A.G., Cambridge University Press, Cambridge.

Lowrie, W., 1990. Identification of ferromagnetic minerals in a rock by coercivity and unblocking temperature properties, *Geoph. Res. Lett.,* **17,** 159–162.

Maiorano, P. & Marino, M., 2004. Calcareous nannofossil bioevents and environmental control on temporal and spatial patterns at the early–middle Pleistocene, *Mar. Micropaleont.,* **53,** 405–422.

Maiorano, P., Marino, M., Di Stefano, E. & Ciaranfi, N., 2004. Calcareous nannofossil events in the lower-middle Pleistocene transition at the Montalbano Jonico section and ODP Site 964d: calibration wih isotope and sapropel stratigraphy, *Riv. Ital. Paleont. Stratigr.,* **110**(2), 547–557.

Mann, S., Sparks, N.H.C., Frankel, R.B., Bazylinski, D.A. & Jannasch, H.W., 1990. Biomineralization of ferrimagnetic greigite (Fe_3S_4) and iron pyrite (FeS_2) in a magnetotactic bacterium, *Nature,* **343,** 258–261.

Mattei, M., Sagnotti, L., Faccenna, C. & Funiciello, R., 1997. Magnetic fabric of weakly deformed clay-rich sediments in the Italian peninsula: relationship with compressional and extensional tectonics, *Tectonophysics,* **271,** 107–122.

Murat, A., 1999. Pliocene-Pleistocene occurrence of sapropel in the western Mediterranean Sea and their relation to eastern Mediterranean sapropels. in *Proceedings of the Ocean Drilling Program, Scientific Results,* Vol. 161, pp. 519–527, eds Zahn, R., Comas, M.C. & Klaus, A., College Station, TX.

Passier, H.F., de Lange, G.J. & Dekkers, M.J., 2001. Magnetic properties and geochemistry of the active oxidation front and the youngest sapropel in the eastern Mediterranean Sea, *Geophys. J. Int.,* **145,** 604–614.

Pierre, C., Belanger, P., Saliège, J.F., Urrutiaguer, M.J. & Murat, A., 1999. Paleoceanography of western Mediterranean during the Pleistocene: oxygen and carbon isotope records at Site 975. in *Proceedings of the Ocean Drilling Program, Scientific Results,* Vol. 161, pp. 481–488, eds Zahn, R., Comas, M.C. & Klaus, A., College Station, TX.

Pike, C.R., Roberts, A.P. & Verosub, K.L., 1999. Characterizing interactions in fine magnetic particle systems using first order reversal curves, *J. appl. Phys.,* **85,** 6660–6667.

Porreca, M., Mattei, M. & Di Vincenzo, G., 2009. Post-deformational growth of late diagenetic greigite in lacustrine sediments from southern Italy, *Geophys. Res. Lett.,* **36,** L09307, doi:10.1029/2009GL037350.

Quidelleur, X., Carlut, J., Soler, V., Valet, J.-P. & Gillot, P.-Y., 2003. The age and duration of the Matuyama-Brunhes transition from new K-Ar data from La Palma (Canary Islands) and revisited 40Ar/39Ar ages, *Earth planet. Sci. Lett.,* **208,** 149–163.

Raffi, I., 2002. Revision of the early–middle Pleistocene calcareous nannofossil biochronology (1.75–0.85 Ma), *Mar. Micropaleontol.,* **45,** 25–55.

Raiswell, R., 1982. Pyrite texture, isotopic composition and the availability of iron. *Am. J. Sci.,* **282,** 1244–1263.

Richmond, G.M., 1996. The INQUA-approved provisional Lower-Middle Pleistocene boundary. in *The Early Middle Pleistocene in Europe,* pp. 319–326, ed. Turner, C., Balkema, Rotterdam.

Richter, C., Roberts, A.P., Stoner, J.S., Benning, L.D. & Chi, C.T., 1998. Magnetostratigraphy of Pliocene–Pleistocene sediments from the eastern Mediterranean Sea, *Proc. ODP, Sci. Res.,* **160,** 61–74.

Roberts, A.P., 1995. Magnetic properties of sedimentary greigite (Fe_3S_4). *Earth planet. Sci. Lett.,* **134,** 227–236.

Roberts, A.P. & Weaver, R., 2005. Multiple mechanisms of remagnetization involving sedimentary greigite (Fe_3S_4). *Earth planet. Sci. Lett.,* **231,** 263–277.

Roberts, A.P., Pike, C.R. & Verosub, K.L., 2000. FORC diagrams: A new tool for characterizing the magnetic properties of natural samples, *J. geophys. Res.,* **105,** 28,461–28,475.

Roberts, A.P., Jiang, W.T., Florindo, F., Horng, C.S. & Laj, C., 2005. Assessing the timing of greigite formation and the reliability of the Upper Olduvai polarity transition record from the Crostolo River, Italy, *Geophys. Res. Lett.,* **32,** L05307, doi:10.1029/2004GL022137.

Roberts, A.P., Liu, Q.S., Rowan, C.J., Chang, L., Carvallo, C., Torrent, J. & Horng, C.S., 2006. Characterization of hematite (a-Fe_2O_3), goethite (a-FeOOH), greigite (Fe_3S_4), and pyrrhotite (Fe_7S_8) using first-order reversal curve diagrams, *J. geophys. Res.,* **111,** B12S35, doi: 10.1029/2006JB004715.

Rochette, P., 1987. Magnetic susceptibility of the rock matrix related to magnetic fabric studies, *J. Struct. Geol.,* **9**(8), 1015–1020.

Rowan, C.J. & Roberts, A.P., 2008. Widespread remagnetizations and a new view of Neogene tectonic rotations within the Australia-Pacific plate boundary zone, New Zealand, *J. geophys. Res.,* **113,** B03103, doi:10.1029/2006JB004594.

Rowan, C.J., Roberts, A.P. & Broadbent, T., 2009. Reductive diagenesis, magnetite dissolution, greigite growth and paleomagnetic smoothing in marine sediments: a new view, *Earth planet. Sci. Lett.,* **277,** 223–235.

Sagnotti, L., 1992. Paleomagnetic evidence for a Pleistocene counterclockwise rotation of the Sant'Arcangelo basin, *Geophys. Res. Lett.,* **19,** 135–138.

Sagnotti, L. & Winkler, A., 1999. Rock magnetism and palaeomagnetism of greigite-bearing mudstones in the Italian peninsula, *Earth planet. Sci. Lett.,* **165,** 67–80.

Sagnotti, L., Speranza, F., Winkler, A., Mattei, M. & Funiciello, R., 1998. Magnetic fabric of clay sediments from the external northern Apennines (Italy), *Phys. Earth planet. Inter.,* **105,** 73–93.

Sagnotti, L., Winkler, A., Alfonsi, L., Florindo, F. & Marra F., 2000. Paleomagnetic constraints on the Plio-Pleistocene geodynamic evolution of the external central-northern Apennines (Italy), *Earth planet. Sci. Lett.,* **180,** 243–257.

Sagnotti, L., Roberts, A.P., Weaver, R., Verosub, K.L., Florindo, F., Pike, C.R., Clayton, T. & Wilson, G.S., 2005. Apparent magnetic polarity reversals due to remagnetization resulting from late diagenetic growth of greigite from siderite, *Geophys. J. Int.,* **160,** 89–100.

Schallreuter, R., 1984. Framboidal pyrite in deep sea sediments, *Init. Repts. DSDP,* **75,** 875–891.

Singer, B.S., Jicha, B.R., Kirby, B.T., Geissman, J.W. & Herrero-Bervera, E., 2008. $^{40}Ar/^{39}Ar$ dating links Albuquerque Volcanoes to the Pringle Falls excursion and the Geomagnetic Instability Time Scale, *Earth planet. Sci. Lett.,* **267,** 584–595.

Snowball, I.F., 1997a. Gyroremanent magnetization and the magnetic properties of greigite-bearing clays in southern Sweden, *Geophys. J. Int.,* **129,** 624–636.

Snowball, I.F., 1997b. The detection of single-domain greigite (Fe_3S_4) using rotational remanent magnetization (RRM) and the effective gyro field (Bg): mineral magnetic and palaeomagnetic applications, *Geophys. J. Int.,* **130,** 704–716.

Speranza, F., Sagnotti, L. & Mattei, M., 1997. Tectonics of the Umbria-Marche-Romagna arc (central northern Apennines, Italy): new paleomagnetic constraints, *J. geophys. Res.,* **102,** 3153–3166.

Speranza, F., Mattei, M., Sagnotti, L. & Grasso, F., 2000. Rotational differences between the northern and southern Tyrrhenian domains: palaeomagnetic constraints from the Amantea basin (Calabria, Italy), *J. geol. Soc. Lond.,* **157,** 327–334.

Stefanelli, S., 2003. Benthic foraminiferal assemblages as tools for paleoenvironmental reconstruction of the early-middle Pleistocene Montalbano Jonico composite section, *Boll. Soc. Paleont. Ital.,* **42,** 281–299.

Stefanelli, S., 2004. Cyclic changes in oxygen based on foraminiferal microhabitats: Early-Middle Pleistocene, Lucania Basin (southern Italy), *J. Micropaleont.,* **23,** 81–95.

Stefanelli, S., Capotondi, L. & Ciaranfi, N., 2005. Foraminiferal record and environmental changes during the deposition of the early-middle Pleistocene sapropels in southern Italy, *Palaeogeog. Palaeclimat. Palaeoecol.,* **216,** 27–52.

Stephenson, A. & Snowball, I.F., 2001. A large gyromagnetic effect in greigite, *Geophys. J. Int.,* **145,** 570–575.

Tauxe, L. & Kent, D., 2004. A simplified statistical model for the geomagnetic field and the detection of shallow bias in paleomagnetic inclinations: Was the ancient magnetic field dipolar?, in *Timescales of the Internal Geomagnetic Field,* Geophys. Monogr. Ser., Vol. 145., pp. 101–115, ed. Channell, J.E.T.C. *et al*., AGU, Washington, DC.

Tauxe, L., Herbert, T., Shackleton, N.J. & Kok, Y.S., 1996. Astronomical calibration of the Matuyama-Brunhes boundary: consequences for magnetic remanence acquisition in marine carbonates and the Asian loess sequences, *Earth planet. Sci. Lett.,* **140,** 133–146.

Thompson, R. & Cameron, T.D.J., 1995. Palaeomagnetic study of Cenozoic sediments in North Sea boreholes: an example of a magnetostratigraphic conundrum in a hydrocarbon producing area, in *Palaeomagnetic Applications in Hydrocarbon Exploration and Production,* Vol. 98, pp. 223–236, eds Turner, P. & Turner, A., Geol. Soc. London Spec. Publ.

Torii, M., Fukuma, K., Horng, C.S. & Lee, T.Q., 1996. Magnetic discrimination of pyrrhotite- and greigite-bearing sediment samples, *Geophys. Res. Lett.,* **23,** 1813–1816.

Vasiliev, I., Franke, C., Meeldijk, J.D., Dekkers, M.J., Langereis, C.G. & Krijgsman, W., 2008. Putative greigite magnetofossils from the Pliocene epoch, *Nat. Geosci.,* **1,** 782–786.

Vandamme, D., 1994. A new method to determine paleosecular variation, *Phys. Earth planet. Inter.,* **85,** 131–142.

Wilkin, R.T. & Barnes, H.L., 1997. Formation processes of framboidal pyrite, *Geochim. Cosmochim. Acta,* **61,** 323–339.

Queries

Journal: GJI
Paper: gji_4480

Dear Author

During the copy-editing of your paper, the following queries arose. Please respond to these by marking up your proofs with the necessary changes/additions. Please write your answers on the query sheet if there is insufficient space on the page proofs. Please write clearly and follow the conventions shown on the corrections sheet. If returning the proof by fax do not write too close to the paper's edge. Please remember that illegible mark-ups may delay publication.

Query Reference	Query	Remarks
Q1	Author: Please check and confirm that you are happy with the section (shown on the right-hand side of the title page) to which this paper has been assigned: a list of all the sections can be found in the Author Guidelines (http://www.wiley.com/bw/submit.asp?ref=0956-540X&site=1).	
Q2	Author: As per journal style only keywords from the keyword list are allowed. No other keywords are allowed, so we have deleted the keywords 'Greigite, Montalbano Jonico section, Early-Middle Pleistocene boundary, Ionian Stage'. Please choose up to six key words from the attached list.	
Q3	Author: A running head short title was not supplied; please check if this one is suitable and, if not, please supply a short title of up to 45 characters that can be used instead.	
Q4	Author: Reference Bickert *et al*. (1997) has not been cited in the text. Please indicate where it should be cited; or delete from the Reference List. Also provide publisher location for the same.	
Q5	Author: Please provide publisher location for reference Ciaranfi *et al*. (1997).	
Q6	Author: Please update reference Ciaranfi *et al*. (2009).	
Q7	Author: Please list all editors if eight or fewer in Reference Comas *et al*. (1996) and also provide publisher details for the same.	
Q8	Author: Please provide publisher details for reference de Kaenel (1999).	
Q9	Author: Reference Laskar *et al*. (2004) has not been cited in the text. Please indicate where it should be cited; or delete from the Reference List.	
Q10	Author: Reference Lisiecki & Raymo (2005) has not been cited in the text. Please indicate where it should be cited; or delete from the Reference List.	
Q11	Author: Please provide publisher details in reference Murat (1999).	

Q12	Author: Please provide publisher details in reference Pierre *et al*. (1999).	

Key words

Authors are requested to choose key words from the list below to describe their work. The key words will be printed underneath the summary and are useful for readers and researchers. Key words should be separated by a semi-colon and listed in the order that they appear in this list. An article should contain no more than six key words.

GEOPHYSICAL METHODS
Time series analysis
Image processing
Neural networks, fuzzy logic
Numerical solutions
Fourier analysis
Wavelet transform
Instability analysis
Inverse theory
Numerical approximations and analysis
Persistence, memory, correlations, clustering
Probabilistic forecasting
Spatial analysis
Downhole methods
Tomography
Interferometry
Thermobarometry
Fractals and multifractals
Non-linear differential equations
Probability distributions
Self-organization

GEODESY and GRAVITY
Satellite geodesy
Reference systems
Sea level change
Space geodetic surveys
Seismic cycle
Transient deformation
Gravity anomalies and Earth structure
Geopotential theory
Time variable gravity
Earth rotation variations
Global change from geodesy
Lunar and planetary geodesy and gravity
Radar interferometry
Plate motions
Tides and planetary waves
Acoustic-gravity waves

GEOMAGNETISM and ELECTROMAGNETISM
Electrical properties
Electromagnetic theory
Magnetotelluric
Non-linear electromagnetics
Archaeomagnetism
Biogenic magnetic minerals
Dynamo: theories and simulations
Environmental magnetism
Geomagnetic excursions
Geomagnetic induction
Ground penetrating radar
Magnetic anomalies: modelling and interpretation
Magnetic and electrical properties
Magnetic fabrics and anisotropy
Magnetic mineralogy and petrology
Magnetostratigraphy
Palaeointensity
Palaeomagnetic secular variation
Palaeomagnetism applied to tectonics
Palaeomagnetism applied to geologic processes
Rapid time variations
Remagnetization
Reversals: process, time scale, magnetostratigraphy
Rock and mineral magnetism
Satellite magnetics
Marine magnetics and palaeomagnetics
Marine electromagnetics

GENERAL SUBJECTS
Geomorphology
Geomechanics
Glaciology
Hydrogeophysics
Ionosphere/atmosphere interactions
Ionosphere/magnetosphere interactions
Gas and hydrate systems
Ocean drilling
Hydrology
Ultra-high pressure metamorphism
Ultra-high temperature metamorphism
Tsunamis
Thermochronology
Heat flow
Hydrothermal systems
Mantle processes
Core, outer core and inner core

COMPOSITION and PHYSICAL PROPERTIES
Microstructures
Permeability and porosity
Plasticity, diffusion, and creep
Composition of the core
Composition of the continental crust
Composition of the oceanic crust
Composition of the mantle
Composition of the planets
Creep and deformation
Defects
Elasticity and anelasticity
Equations of state
High-pressure behaviour
Fracture and flow
Friction
Fault zone rheology
Phase transitions

SEISMOLOGY
Controlled source seismology
Earthquake dynamics
Earthquake ground motions
Earthquake source observations
Seismic monitoring and test-ban treaty verification
Palaeoseismology
Earthquake interaction, forecasting, and prediction
Seismicity and tectonics
Body waves
Surface waves and free oscillations
Interface waves
Guided waves
Coda waves
Seismic anisotropy
Seismic attenuation
Site effects
Seismic tomography
Volcano seismology
Computational seismology
Theoretical seismology
Statistical seismology
Wave scattering and diffraction
Wave propagation
Acoustic properties
Early warning
Rheology and friction of fault zones

TECTONOPHYSICS
Planetary tectonics
Mid-ocean ridge processes
Transform faults
Subduction zone processes
Intra-plate processes
Volcanic arc processes
Back-arc basin processes
Cratons
Continental margins: convergent
Continental margins: divergent
Continental margins: transform
Continental neotectonics
Continental tectonics: compressional
Continental tectonics: extensional
Continental tectonics: strike-slip and transform
Sedimentary basin processes
Oceanic hotspots and intraplate volcanism
Oceanic plateaus and microcontinents
Oceanic transform and fracture zone processes
Submarine landslides
Submarine tectonics and volcanism
Tectonics and landscape evolution
Tectonics and climatic interactions
Dynamics and mechanics of faulting
Dynamics of lithosphere and mantle
Dynamics: convection currents, and mantle plumes
Dynamics: gravity and tectonics
Dynamics: seismotectonics
Heat generation and transport

Impact phenomena
Hotspots
Large igneous provinces
Lithospheric flexure
Obduction tectonics
Neotectonics
Diapir and diapirism
Folds and folding
Fractures and faults
Kinematics of crustal and mantle deformation
High strain deformation zones
Crustal structure
Mechanics, theory, and modelling
Rheology: crust and lithosphere
Rheology: mantle

PLANETS
Planetary interiors
Planetary volcanism

VOLCANOLOGY
Physics of magma and magma bodies
Magma chamber processes
Magma genesis and partial melting
Pluton emplacement
Effusive volcanism
Mud volcanism
Subaqueous volcanism
Explosive volcanism
Volcaniclastic deposits
Volcano/climate interactions
Atmospheric effects (volcano)
Volcanic gases
Lava rheology and morphology
Magma migration and fragmentation
Eruption mechanisms and flow emplacement
Physics and chemistry of magma bodies
Calderas
Experimental volcanism
Tephrochronology
Remote sensing of volcanoes
Volcano monitoring
Volcanic hazards and risks

GEOGRAPHIC LOCATION
Africa
Antarctica
Arctic region
Asia
Atlantic Ocean
Australia
Europe
Indian Ocean
New Zealand
North America
Pacific Ocean
South America

MARKED PROOF

Please correct and return this set

Please use the proof correction marks shown below for all alterations and corrections. If you wish to return your proof by fax you should ensure that all amendments are written clearly in dark ink and are made well within the page margins.

Instruction to printer	*Textual mark*	*Marginal mark*
Leave unchanged	... under matter to remain	
Insert in text the matter indicated in the margin		New matter followed by or
Delete	through single character, rule or underline or through all characters to be deleted	or
Substitute character or substitute part of one or more word(s)	through letter or through characters	new character or new characters
Change to italics	under matter to be changed	
Change to capitals	under matter to be changed	
Change to small capitals	under matter to be changed	
Change to bold type	under matter to be changed	
Change to bold italic	under matter to be changed	
Change to lower case	Encircle matter to be changed	
Change italic to upright type	(As above)	
Change bold to non-bold type	(As above)	
Insert 'superior' character	through character or where required	or under character e.g. or
Insert 'inferior' character	(As above)	over character e.g.
Insert full stop	(As above)	
Insert comma	(As above)	,
Insert single quotation marks	(As above)	or and/or or
Insert double quotation marks	(As above)	or and/or or
Insert hyphen	(As above)	
Start new paragraph		
No new paragraph		
Transpose		
Close up	linking characters	
Insert or substitute space between characters or words	through character or where required	
Reduce space between characters or words	between characters or words affected	